J. Fluid Mech. (2005), *vol.* 535, *pp.* 415–443.
doi:10.1017/S002211200500501X Printed in the United Kingdom

Boundary-layer separation control on a thin airfoil using local suction

By H. ATIK[1], C.-Y. KIM[2], L. L. VAN DOMMELEN[3] AND J. D. A. WALKER[2]†

[1]The Scientific & Technical Research Council, Defense Industries Research & Development Institute, P.K.16 Mamak, Ankara, Turkey 06261

[2]Department of Mechanical Engineering and Mechanics, Lehigh University, 19 Memorial Drive West, Bethlehem, PA 18015, USA

[3]Department of Mechanical Engineering, Florida A&M and Florida State Universities, Tallahassee, FL 32310, USA

(Received 17 June 2002 and in revised form 28 February 2005)

High-speed incompressible flow past a thin airfoil in a uniform stream is considered. When the angle of attack for a solid airfoil exceeds a certain critical value, the boundary layer in the leading-edge region separates in a process known to lead to dynamic stall. Here suction near the leading edge is studied as a means of controlling separation and thereby inhibiting dynamic stall. First, steady boundary-layer solutions are obtained to determine the nature of suction distributions required to suppress separation on an airfoil at an angle of attack beyond the critical value (for a solid wall). Unsteady boundary-layer solutions are then obtained, using a combination of Eulerian and Lagrangian techniques, for an airfoil at an angle of attack exceeding the critical value; the effects of various parameters associated with the finite-length suction slot, its location and the suction strength are considered. Major modifications of the Lagrangian numerical method are required to account for suction at the wall. It is determined that substantial delays in separation can be achieved even when the suction is weak, provided that the suction is initiated at an early stage.

1. Introduction

Dynamic stall is a term used to describe a process in which flow separation occurs on an airfoil oriented at a sufficiently high angle of attack in a uniform flow. Different types of stall have been identified in the past (see, for example, McCullough & Gault 1951; McAlister & Carr 1979; Currier & Fung 1992) but the most important type for thin airfoils occurs in the leading-edge region (Currier & Fung 1992; Acharya & Metwally 1992; Shih *et al.* 1992; Shih, Lourenco & Krothpalli 1995) when the flow is at high Reynolds number *Re*. Leading-edge stall is generally preceded by laminar boundary-layer separation near the airfoil nose. At high *Re*, separation is a strongly interactive event wherein the boundary layer erupts from the surface in a sharply focused narrow plume; the onset of this process was first identified by Van Dommelen & Shen (1980, 1982) and subsequently described by other authors (see, for example, Cowley 1983; Elliott, Cowley & Smith 1983; Peridier, Smith & Walker 1991; Cowley, Van Dommelen & Lam 1990). Doligalski, Smith & Walker

† Professor Walker passed away in March 2004.

(1994) argue that leading-edge separation initiates the dynamic stall process in which a vortex is quickly created above the upper surface of the airfoil. While the stall vortex is resident above the airfoil, significant increases in lift are experienced, compared to the steady-flow maximum value (Ham 1968; Francis & Keesee 1985). However, this extra lift is normally short-lived since the stall vortex induces a second separation process in the boundary layer near mid-chord that quickly leads to detachment of the vortex. As the stall vortex convects into the airfoil wake, a substantial penalty is paid in terms of a sharp decrease in lift, accompanied by an abrupt pitching moment.

In recent times, dynamic stall has received increasing attention in connection with future designs for helicopters and combat aircraft. Experimental observations of certain unsteady airfoil motions show that angles of attack well beyond the static stall angle can be attained without provoking breakaway separation (at least for a brief interval). The static stall angle may be regarded as the minimum angle of attack for which stall occurs from a stationary airfoil in uniform flow. In practice, the measured lift on an airfoil grows linearly with small angles of attack and the static stall angle is defined (somewhat subjectively) as the first angle for which a significant deviation from the linear relationship is observed. This definition is not necessarily synonymous with the first onset of separation. With increasing angle of attack, a short bubble of recirculating flow is first observed near the nose and experiments suggest that this event does not produce an appreciable deviation from the linear lift/incidence relationship; however at higher angles, unsteady breakaway separation is observed. It appears that relatively high lift can be achieved in unsteady flow (at least for short periods) and Francis & Keesee (1985) were able to briefly obtain lift values up to thrice the maximum static lift using an airfoil pitched up rapidly in a uniform flow. This phenomenon is attractive since it suggests that higher values of lift, and thus increased manoeuvrability, could be realized in aeronautical applications. For example, rotorcraft blades are configured to pitch up rapidly as each blade on the main rotor moves in a direction opposite to the forward motion of the helicopter (the retreating side) in order to balance the lift on the advancing side, where a relatively higher mainstream speed is encountered. Although enhanced lift can be achieved as the blade is pitched above the static stall angle, it has been difficult to exploit the phenomenon due to the severe penalty that must eventually be paid when the stall vortex leaves the upper surface of the blade. For this reason, current helicopters are designed to try to avoid the dynamic stall regime insofar as this is possible. It is likely, however, that future designs of rotorcraft could achieve substantial gains in manoeuvrability and much recent work has concerned various ways to control the leading-edge separation (see, for example, Karim & Acharya 1994; Wang 1995; Yu *et al.* 1995; Alrefai & Acharya 1996).

To gain advantage in air-to-air combat, manoeuvrability is generally believed to be more important than speed and for brief periods, the wings of a fighter aircraft could be at angles of attack up to 75° (Francis 1995). Thus the operating environment is at times deep within an unsteady regime where the airfoil would normally stall in steady flow and control mechanisms must be considered to avoid abrupt loss of lift and the potential instabilities associated with unsteady flow. A common feature of combat aircraft and rotorcraft is that the airfoil manoeuvres which penetrate the unsteady regime are rapid and often of relatively short duration. Thus practical control measures that inhibit separation from the leading-edge region are of considerable interest, in order that the process leading to dynamic stall may be delayed (and potentially suppressed), whilst still maintaining enhanced levels of lift.

The issue of boundary-layer control at the leading edge is difficult in a practical sense, especially for helicopter blades, where complex mechanical control surfaces do not seem feasible. In the past, suction has been used for control and, for example, Poppleton (1955) showed that weak suction applied over the first 15% of chord on the upper surface could produce a 40% increase in lift for an airfoil at 15° angle of attack. More recently, Karim & Acharya (1994) and Alrefai & Acharya (1996) have carried out experiments with a small suction slot over the first 2% to 5% of chord, for Reynolds numbers Re_c (based on chord length c) up to around 10^5; the airfoil was pitched up to angles of attack approaching 35°, and thus was within the post-stall regime. It was found that leading-edge separation was inhibited, and in some cases, the dynamic stall process was suppressed. Wang (1995) has carried out numerical solutions of the Navier–Stokes equations at $Re_c = 5000$ using a vortex method. For uniform suction in the slot, the most effective configuration was similar to that studied by Poppleton (1955), wherein the slot extended over the first 20% of chord for an NACA 0012 airfoil. The airfoil was pitched up uniformly from rest to angles in excess of 30°. It was determined that if the suction was applied early enough, leading-edge separation and dynamic stall could be effectively prevented, while enhanced lift was still realized.

In an earlier partial study, similar conclusions were reached by Shen and Xiao (S. F. Shen, 1990, private communication) concerning the effectiveness of suction as a separation control on the rear half of an impulsively started circular cylinder. For a solid wall, the boundary-layer solution reaches a separation singularity at a time of $t^* \approx 1.5 r_0^*/U_0$, where r_0^* is the cylinder radius and U_0 the free-stream velocity. When a suction distribution of the form $v_r(\theta, r_0^*, t^*) = -\bar{V}\cos(\theta - \pi/4)\sqrt{U_0 \nu / r_0^*}$ was applied for $0 \leqslant \theta \leqslant \pi/2$ (θ is measured from the downstream radius and ν is the viscosity) starting at $t^* = 1.05 r_0^*/U_0$, separation could be suppressed during the considered time interval for sufficiently large values of $\bar{V} \approx 10$. The results for other cases considered indicated that more suction was required to suppress separation when suction is started later, and for a narrower slot.

In view of the previous work, the central focus here is on the leading-edge region of the airfoil and the primary purpose is to investigate the question of what can be done to avoid separation in transient flows.† In the present study, a suction slot was introduced on the upper surface of the parabola with a total suction volumetric rate $O(\varepsilon Re_c^{-1/2})$, where ε is the airfoil thickness ratio (defined as the maximum thickness divided by c). Experience shows that a Lagrangian solution is necessary for an accurate and reliable determination of the Van Dommelen & Shen (1980) singularity but because there are no existing schemes to account for suction, a method is developed in §6. As results were being obtained, it seemed there was a lack of basic knowledge, which was required to embed the unsteady computations in a larger context. For example, even in steady flow, there was a question of whether separation could be avoided for any angle of attack by an appropriate amount of suction and if so, how much suction was needed. In addition should the suction be applied locally with a narrow slot or would it be more desirable to distribute the suction over a larger area (to be determined)? Some answers to these questions are given in §4.

† Here 'separation' implies that a smooth thin boundary layer fails to exist. Separation will not occur if the Goldstein (1948) and Van Dommelen & Shen (1980) singularities can be avoided in steady and unsteady flow, respectively. Flow reversal does not necessarily imply that the boundary-layer solution terminates in unsteady flow (Sears & Telionis 1975).

The case of primary interest is the transient flow in the nose region when the scaled angle of attack changes due to alterations in the incoming flow. The flow change is assumed to be initiated impulsively, corresponding most directly to a sudden gust or a sudden initiation of rotation of the airfoil section about some suitable axis. It is further assumed that the entire flow is impulsively started from rest, as is common in this type of study; the reason is that this initial condition is cleaner than an arbitrary assumption of some type of pre-existing boundary layer, which would also lead to the complication of a two-layer structure at early times. It seems unlikely that a thin attached initial boundary layer will fundamentally change any of the processes involved.

The analysis assumes laminar flow in the leading-edge region, which is believed to be of significant practical utility. While as one referee has pointed out, the boundary layer may be very unstable after flow reversal see (Cowley, Hocking & Tutty 1985), in the transient situations considered, disturbances have only a limited time to grow. Although turbulence may be observed experimentally downstream of the nose, it is unclear whether a turbulence model (to characterize small fluctuations in a possible transitional zone) will have a dramatic influence on the Van Dommelen & Shen process, which is driven by the convective terms. In any event, it is believed to be important to understand the laminar problem before the turbulent equivalent is addressed. In the present study, it was found that the separation process could be significantly delayed at all finite scaled angles of attack, and under the right circumstances completely eliminated.

2. Governing equations

Consider an airfoil of thickness ratio ε which is immersed in a uniform flow of speed U_0 and which is thin in the sense that $\varepsilon \ll 1$. When the airfoil executes a manoeuvre such that the angle of attack is $O(\varepsilon)$, the inviscid flow field may be determined using thin airfoil theory. For a given airfoil shape with a smooth nose, the inviscid solution describing the perturbation tangential velocity (about the uniform flow) is singular at the leading edge. This solution is interpreted as an outer solution, which must be matched to an appropriate solution in the leading-edge region (see, for example, Van Dyke 1956, 1964; Katz & Plotkin 1991). The nose of the airfoil can be represented by a parabola with a dimensionless nose radius r_0 (referred to $c/2$), given by $r_0 = R_0\varepsilon^2$. Here R_0 is an $O(1)$ constant and, for example, $R_0 = 2.204$ for an NACA 0012 airfoil ($\varepsilon = 0.12$) and $R_0 = 2.370$ for a Joukowsky airfoil (Katz & Plotkin 1991). Let x' and y' denote dimensionless scaled Cartesian coordinates (referred to the nose radius) centred at the parabola vertex $y' = \pm\sqrt{2x'}$.

The inviscid motion around the parabola can be conveniently described in terms of parabolic coordinates $(\tilde{\xi}, \tilde{\eta})$ defined by

$$x' + \mathrm{i}y' = \tfrac{1}{2} + \tfrac{1}{2}\left\{\tilde{\xi} + \mathrm{i}(\tilde{\eta} + 1)\right\}^2. \tag{2.1}$$

The parabola surface is $\tilde{\eta} = 0$ and $\tilde{\xi}$ varies from $-\infty$ to $+\infty$ on the surface. It can be shown (Van Dyke 1956, 1964) that the inviscid slip velocity U_∞ (referred to U_0) is

$$U_\infty(\tilde{\xi}, t) = \frac{\tilde{\xi} + a}{\sqrt{\tilde{\xi}^2 + 1}} \tag{2.2}$$

where a can be a specified function of time whose value is proportional to the effective angle of attack for the flow near the nose, including the effects of Kutta condition, camber, motion, and ambient flow changes, divided by the square root of

the non-dimensional nose radius r_0 (see, for example, Wang 1995). The function $a(t)$ can be determined by matching the leading-edge solution to the global airfoil solution for a given shape and manoeuvre (Zalutsky 2000). The stagnation point is the point of attachment of the inviscid flow and occurs on the lower surface of the parabola (for $a(t) > 0$) at $\tilde{\xi} = -a$.

The boundary-layer problem can be formulated in terms of the parabolic coordinates by introducing a scaled normal coordinate and velocity $\tilde{y} = Re_r^{1/2}\tilde{\eta}$, $\tilde{v} = Re_r^{1/2}\tilde{u}_{\tilde{\eta}}$, respectively, where $\tilde{u}_{\tilde{\eta}}$ is the velocity component in the $\tilde{\eta}$-direction (referred to U_0) and $Re_r = r_0 c U_0/2\nu$ is the Reynolds number based on the nose radius, which is assumed large. It is convenient to introduce new coordinates and a redefined normal velocity by

$$x = \tfrac{1}{2}\{\tilde{\xi}(1+\tilde{\xi}^2)^{1/2} + \sinh^{-1}\tilde{\xi}\}, \quad y = (\tilde{\xi}^2+1)^{1/2}\tilde{y}, \quad u = \tilde{u}_{\tilde{\xi}}, \quad v = \tilde{v} + \frac{\tilde{\xi}\tilde{y}}{(\tilde{\xi}^2+1)^{3/2}}u, \tag{2.3}$$

where x measures arclength from the vertex (referred to the nose radius). The Eulerian boundary-layer equations are

$$\frac{\partial u}{\partial t} + u\frac{\partial u}{\partial x} + v\frac{\partial u}{\partial y} = -\frac{\partial p_\infty}{\partial x} + \frac{\partial^2 u}{\partial y^2}, \qquad \frac{\partial u}{\partial x} + \frac{\partial v}{\partial y} = 0, \tag{2.4}$$

where

$$\frac{\partial p_\infty}{\partial x} \equiv -\frac{\partial U_\infty}{\partial t} - U_\infty \frac{\partial U_\infty}{\partial \tilde{\xi}}\frac{\mathrm{d}\tilde{\xi}}{\mathrm{d}x} \tag{2.5}$$

is equal to the non-dimensional pressure gradient, assuming that non-inertial terms, if any, can be ignored compared to the large convective terms (White 1991, p. 95). The boundary conditions are

$$u \to U_\infty(\tilde{\xi}(x), t) \quad \text{as} \quad y \to \infty; \quad u = u_w(x,t), \quad v = v_w(x,t) \quad \text{at} \quad y = 0, \tag{2.6}$$

where u_w and v_w represent the imposed surface velocities.

It is well known that for positive constant a less than a critical value of $a_c \approx 1.16$ (Werle & Davis 1972; Cebeci, Khattab & Stewartson 1980; Ruban 1981), a steady attached boundary-layer solution exists. (A more precise value of a_c will be obtained here in § 3.) The inviscid flow on the pressure side of the parabola accelerates smoothly and the boundary layer evolves to the Blasius solution as $\tilde{\xi} \to -\infty$. On the other hand, the inviscid flow is accelerated around the nose, reaching a maximum on the upper surface at $\tilde{\xi} = 1/a$. Thereafter the pressure gradient is adverse, and the wall shear decreases to a positive minimum if a is somewhat less than a_c; the boundary layer then recovers, eventually approaching a Blasius profile downstream as $\tilde{\xi} \to \infty$. At the critical value a_c, the minimum in wall shear is identically zero at $x \approx 6.8$ (see § 3 for a refined value). Within a small range $O(Re_r^{-2/5})$ of values of a near a_c, Ruban (1981) and Stewartson, Smith & Kaups (1982, equation 3.19) have shown that a family of steady solutions exists describing a short bubble of reversed flow. This phenomenon is known as marginal separation. Once a exceeds a_c by an amount $O(1)$, no matter how small, Degani, Li & Walker (1996) show that unsteady boundary-layer separation (and a local eruption) occurs in the leading-edge region.

If design conditions for aerodynamic surfaces are configured to avoid separation entirely, then the angle of attack (and hence the lift) is restricted to relatively low values. For example, the critical value for steady flow for a NACA 0012 airfoil is 5.89° and for a Joukowsky airfoil 6.12° (for $\varepsilon = 0.12$); for an abrupt start, these angles are

doubled. Note that the static stall angle for the NACA 0012 airfoil is larger than the former value and estimates from experiments range from 14° to 18°. There are several possible reasons for this. First the laminar flow at the leading edge may separate just above the critical angle and provoke early transition; the turbulent boundary layer can then subsequently re-attach downstream and in such a situation the observed lift would still roughly conform to the linear relation with angle of attack. It is also possible that 'finite thickness effects' play an important role for the NACA 0012 airfoil; for example, at about 3.5% of chord the deviation of the parabola is about 10% in excess of the actual airfoil thickness. Wang (1995) noted significant deviations between Navier–Stokes simulations of a NACA 0012 airfoil for $Re_c = 5000$ and the corresponding approximating parabolic nose at $Re_r = 79$. The objective of the present work, however, is not to model a specific airfoil shape closely but to determine if the limits on angle of attack can be substantially expanded through leading-edge suction.

The reason that suction can be effective for inhibiting separation may be inferred from the streamwise momentum equation (2.4). If $\omega = -\partial u/\partial y$ denotes the scaled boundary-layer vorticity (with respect to $2U_0 Re_r^{1/2}/r_0 c$), the scaled surface vorticity flux (Lighthill 1963) is

$$q_w = -\left.\frac{\partial \omega}{\partial y}\right|_{y=0} = \frac{\partial p_\infty}{\partial x} - v_w(x,t)\omega(x,0,t), \tag{2.7}$$

for $u_w = 0$. Suppose that at some initial time, an unseparated flow exists with $u > 0$ and $\omega < 0$ throughout the boundary layer for $\tilde{\xi} > -a$ and then an impulsive manoeuvre of the airfoil or ambient flow change increases the effective angle of attack to some value $a_o > a_c$. The new inviscid flow achieves an absolute maximum of $U_{\infty,m}$ at $\tilde{\xi}_m = 1/a_o$ and for $\tilde{\xi} > \tilde{\xi}_m$, the pressure gradient is adverse. For a solid wall, the vorticity flux on the major part of the upper surface is positive and just downstream of $\tilde{\xi}_m$, where the pressure is increasing most rapidly, a large amount of positive vorticity is soon created. Thus a line of zero vorticity progressively penetrates into a region of otherwise negative vorticity. It is somewhere along this line that the Van Dommelen & Shen (1980, 1982) process is born. It is evident from equation (2.7) that if suction is applied at the wall ($v_w < 0$) while $\omega(x,0,t)$ is still negative, then the suction provides a counteracting negative vorticity flux. This control can, in principle, be effective at suppressing separation, depending on the magnitude of v_w and whether the suction is initiated at sufficiently early times.

Now let a suction slot be located on a section of the wall from $x = x_0$ to $x = x_1$, where x_0, x_1 are constants. A number of suction distributions were considered in this study, but for the majority of the calculations the following form was used:

$$v_w = v(x,0,t) = -V \sin^i q, \quad q = \frac{(x - x_0)\pi}{(x_1 - x_0)}, \tag{2.8}$$

where i is a chosen integer and V is the maximum scaled suction velocity. For uniform suction $i = 0$ and $v(x,0,t)$ is discontinuous at the edges of the slot. In most of the unsteady calculations, a higher value for i was selected to ensure a smoother transition at the edges of the slot; derivatives up to order $(i-1)$ are continuous there.

A dimensionless suction coefficient can be defined as the rate of volume removal divided by $U_0 r_0 c/2$ according to

$$c_q = Re_r^{-1/2} \int_{x_0}^{x_1} |v(x,0,t)|\, \mathrm{d}x = Re_r^{-1/2} C_Q, \tag{2.9}$$

where it is easily shown that $C_Q = V(x_1 - x_0)e_i$; for $i = 0, 1, \ldots 4$, the values of e_i are $1, 2/\pi, 1/2, 4/3\pi$ and $3/8$ respectively.

To assess whether weak suction through a slot can significantly inhibit separation in the limit $Re_r \to \infty$, a representative base flow must be selected. First note that in addition to the time t (referred to U_0 and the nose radius), there is also a global dimensionless time $\bar{t}$ (referred to the chord) such that $\bar{t} = R_0\varepsilon^2 t/2$. Thus a time interval that is $O(1)$ in $\bar{t}$ is effectively infinite in the nose time t (for thin airfoils). This means that an airfoil manoeuvre on the global scale will produce an effectively steady flow near the nose for $a < a_c$ and separation will be almost immediate for any angle of attack such that $a - a_c > 0$. Various manoeuvres that take place on the 'short' time scale could be addressed. However, here the simplest situation where a suddenly achieves a constant value is considered; this is believed to be representative of the worst possible case for a separation control to be effective. From a physical standpoint, this may be viewed as a thin airfoil which is abruptly started at a small angle of attack at $t = 0$; the determination of the unsteady inviscid flow is known as the Wagner (1925) problem when the trailing edge is cusped. For steady flow satisfying the Kutta condition, matching of the global inviscid solution to the local inviscid nose solution yields an angle of attack, measured from the direction of symmetric flow around the nose, $\alpha^* = \frac{1}{2}R_0^{1/2}\varepsilon a$ (Degani *et al.* 1996). For unsteady flow, the solution of the Wagner (1925) problem (see, for example, Zalutsky 2000) predicts that the value of a achieves one-half of its final value abruptly at $t = 0$, since the circulation around the steady airfoil increases a by a factor 2. Since the frontal stagnation point moves along the leading edge with the slow time scale $\bar{t}$ as the airfoil sheds vorticity and hence picks up circulation, $\alpha^* = R_0^{1/2}\varepsilon a$ on the time scale studied here. This is consistent with experimental observations that relatively high angles of attack can be achieved in unsteady flow, as opposed to steady flow, without rapidly provoking separation at the leading edge. We will now first examine the effect of steady suction on this flow.

3. Steady numerical scheme

Calculations were carried out for steady flow to form a basis of comparison for the unsteady computations, as well as to determine minimal suction distributions required to eliminate separation. Steady boundary-layer calculations were initiated at the stagnation point $\tilde{\xi} = -a$ and continued downstream over the top surface. A vorticity formulation, previously used by one of us (L.v.D.) in unsteady second-order (Van Dyke 1964) boundary-layer computations, was employed. Advantages of this approach are that: (i) it is easier to implement boundary conditions for large y numerically, especially at second-order, and (ii) wall boundary conditions on the vorticity can be enforced exactly. The vorticity $\omega = -\partial u/\partial y$ satisfies

$$\frac{\partial \omega}{\partial t} + u\frac{\partial \omega}{\partial x} + v\frac{\partial \omega}{\partial y} = \frac{\partial^2 \omega}{\partial y^2}, \quad \int_0^\infty \omega \, \mathrm{d}y = -U_\infty(x), \quad \omega \to 0 \quad \text{as} \quad y \to \infty. \tag{3.1}$$

Equation (2.7) relates $\partial\omega/\partial y$ and ω at $y = 0$ to the pressure gradient but using the integral condition in (3.1) ensures that the external flow velocity at large y remains correct regardless of numerical errors. Such integral conditions have been used with good success in other contexts (see, for example, Collins & Dennis 1973).

The numerical method used is a Crank–Nicholson type scheme. A mapping of y to a computational coordinate $\hat{y}$, of the form $y = k_y \tan(\pi\hat{y}/2)$, was used to define a non-uniform mesh in y using a uniform spacing in $\hat{y}$. A value $k_y = 1.33\bar{\delta}^*(x)$ was selected,

with $\bar{\delta}^*(x)$ being a rough least-squares approximation to preliminary values of the displacement thickness (including a growth proportional to $\sqrt{x}$ far downstream). In the x-direction, another non-uniform mapping $x = k_x \tan(A_0 + A_1\hat{x})$ was used, with k_x a mesh-stretching parameter, typically chosen to be 2 or 3; A_0 and A_1 were chosen to locate the stagnation point at $\hat{x} = 0$ and produce infinite x at $\hat{x} = 1$. Differencing of the viscous term was done in physical space in order that quadratic velocity profiles were differenced exactly regardless of the mapping from y to $\hat{y}$. The y-derivatives in the relationship between u and ω and in the continuity equation were treated similarly; in particular, near the external flow region where v is $O(y)$ as $y \to \infty$, the integration is exact regardless of the strong mesh stretching.

Situations were considered where either the normal velocity or the wall shear was prescribed; whichever was specified left the other unknown. At any x-station, the nonlinear Crank–Nicholson equations were solved using Newton iteration, requiring a system of block-tridiagonal linear equations to be solved at each iteration if the unknown wall boundary is handled through a shooting method. Because of linearity, the shooting method converges in one step. Typically five to ten Newton iterations were required to produce convergence to round-off error.

For a given value of a, the calculation was continued until the entire paraboloid had been computed or until a Goldstein (1948) singularity was encountered. This singularity evolves when the pressure distribution is prescribed and the wall shear tends to zero; its occurrence has been classically referred to as *steady separation* and continuation of the integration downstream is not then possible. The four-term analytical expansion of the wall shear, as generalized by Terrill (1960) to include suction, was used in some computations to extrapolate the location of the separation singularity from the data just upstream; this procedure avoids some numerical error provoked by the singular behaviour at the separation point itself. Computations were repeated at varying mesh sizes to ensure that all presented results are mesh independent. Reasonable accuracy was usually achieved with 128 or 256 mesh points in each direction, but most final results were obtained with 2048 or 4096 mesh points. The circular cylinder flow of Terrill (1960) was recomputed as a test and excellent agreement was obtained.

At the edges of the suction slot where an abrupt change in suction velocity occurs, the usual algebraic singularities and a two-layer structure occur (see, for example, Rosenhead 1963; Walker & Dennis 1972; Smith & Stewartson 1973). Following well-known methods and omitting the details, suppose a change in suction velocity occurs at $x = x_e$, by an amount $\Delta v_w \equiv v_w^+ - v_w^-$, where the sign denotes values of v_w just downstream and upstream of x_e. Downstream of x_e a viscous sublayer of extent $y = O(\bar{x}^{1/3})$ forms (where $\bar{x} = x - x_e$), with the usual transposed main boundary layer above it. The sublayer flow is readily solved in terms of incomplete Gamma functions and it is found that the scaled wall shear behaves as

$$\tau_w = -\omega(x, 0) = \tau_e - \frac{3^{5/6}\tau_e^{2/3}\Gamma(2/3)d_1}{\pi}\Delta v_w \bar{x}^{1/3} + \cdots, \tag{3.2}$$

immediately beyond the edge, with τ_e the wall shear of the boundary layer immediately before the edge and $d_1 = \pi/(3^{1/6}\Gamma^2(2/3))$. Similarly the displacement thickness and displacement velocity at the boundary-layer edge show irregular behaviour according to

$$\delta^*(x) = \delta^*(x_e) + d_1\tau_e^{-2/3}\Delta v_w \bar{x}^{2/3} + \cdots, \quad v_d \sim \tfrac{2}{3}\left(\bar{x}\tau_e^2\right)^{-1/3} d_1 U_\infty(x_e)\Delta v_w + \cdots, \tag{3.3}$$

for $\bar{x} \ll 1$.

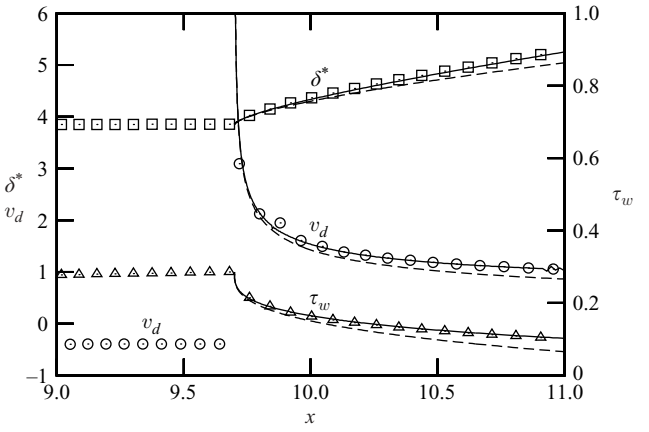

FIGURE 1. Effect of not resolving the two-layer structure; numerical results for wall shear (△), displacement thickness (□), and displacement velocity (○).

A very complex code was developed that actually resolved the two-layer structure (see also Smith & Stewartson 1973). However, it was found that the basic scheme works well either if the jump was represented as a smooth but rapid transition over a small streamwise region or if a simple backward difference was used for one or two steps after an abrupt jump (see also Walker & Dennis 1972). Calculated results (for a case where suction terminates at $x = 9.7$) using the latter approach with two backward Euler steps are shown by symbols in figure 1; corresponding results with the complex code (which still has visible stability problems downstream) are shown as solid lines. The asymptotic results (3.2)–(3.3) are shown as broken lines. (The resolved code does not use the asymptotic solution and thus provides a true test of it). The infinite displacement velocity cannot be correctly captured by the unresolved scheme, but evidently the effects disappear after a few steps, and away from the jump, convergence with mesh size remained unaffected even for the unsmoothed computations. The singularity induced by the jump in the normal velocity can, in principle, be resolved by a triple-deck structure on the edges of the slot; these local interaction regions, however, do not affect the downstream results.

To further validate the scheme, the critical angle of attack at which separation first occurs was recomputed. A refined value of $a_c = 1.15755$ was determined using extrapolation of the minimum shear, and a more precise value of 1.15757 by directly shooting for zero shear, at $x = 6.823$. These values of a_c agree with Werle & Davis (1972), who indicate that $1.157 < a_c < 1.158$, as well as subsequent estimates by Cebeci *et al.* (1980) of 1.155 and Ruban (1981) of 1.1556. The separation location at $x = 6.823$ corresponds to $\tilde{\xi} = 3.351$. This agrees with value $\tilde{\xi} \approx 3.34$ read off (by us, as 10.1 for the Görtler variable) from the corresponding graph in Werle & Davis (1972), with the value $\tilde{\xi} \approx 3.3$ estimated by Stewartson *et al.* (1982) apparently using data from Cebeci *et al.* (1980), and with $x = 6.99$ found by Ruban (1981).

4. Calculated steady results

Various computations were carried out to determine if a finite amount of scaled suction, i.e. a physical volumetric suction rate $O(\varepsilon^2 Re_r^{-1/2})$, applied in a variety of ways, could eliminate steady separation. The first implementation of suction considered is referred to as '*locally-minimal suction*' and just enough suction was applied at each

a/Ω_m	0.2	0.1	0.5	0.025	0
2	2.5845	2.3974	2.3568	2.3471	(2.3439)
3	6.1721	5.8868	5.8247	5.8099	(5.8050)
4	9.953	9.570	9.486	9.466	(9.459)

TABLE 1. Scaled suction coefficient C_Q for various a and Ω_m for 'locally minimal' suction.

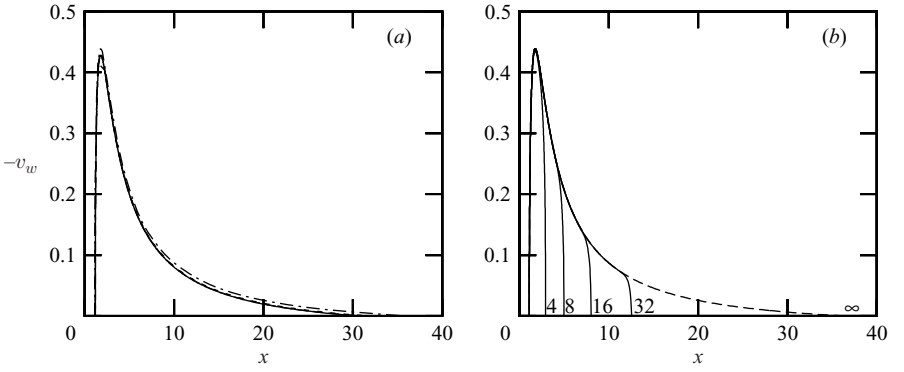

FIGURE 2. 'Locally minimal' suction profiles for $a=2$. Steady profiles (a) are for $\Omega_m=0.025$ (solid line), 0.05 (long dash), 0.1 (short dash), and 0.2 (short/long dash) (curves at smaller values coincide). Unsteady profiles (b) are for $\Omega_m=0.2$ and times $t=4$, 8, 16, 32 (solid lines) and ∞ (dash).

x-station to ensure that the non-dimensional wall vorticity parameter

$$\Omega \equiv \frac{u_y(x,0)}{U_\infty(x)}\delta^*(x) \geqslant \Omega_m, \tag{4.1}$$

where δ^* is the displacement thickness and Ω_m is a chosen tolerance level. Ω is dimensionless and depends only on the velocity profile; for the asymptotic suction profile $\Omega=1$ (Rosenhead 1963), while $\Omega=0.571$ for the Blasius profile. Finite suction cannot occur for $\Omega_m>0.571$, since u must approach the Blasius solution as $x\to\infty$.

Calculations were started at the front stagnation point and once Ω threatened to drop below the specified value of Ω_m in the region of adverse pressure gradient on the upper surface, just enough suction was introduced at that x to maintain condition (4.1). Such a suction distribution is admittedly difficult to implement in practice but is useful in establishing the minimum suction volumes required to avoid separation. Computed suction coefficients for various Ω_m and a are given in table 1. The last column gives apparent limiting values as $\Omega_m\to 0$, which are conjectured to be the minimum suction amounts required to avoid separation for each a. The required suction increases fairly linearly with $a-a_c$.

Computed suction profiles on the upper surface for $a=2$ and various Ω_m are shown in figure 2(a). Evidently the suction must be continued relatively far downstream but the profiles are almost the same for all Ω_m.

The suction profiles for the corresponding unsteady problem (with the flow impulsively started from rest) and using $\Omega_m=0.2$, are shown in figure 2(b). It may be observed that the long tail to the suction distribution only becomes necessary for numerically very large times; at earlier times, the suction volume is much reduced from the steady requirement.

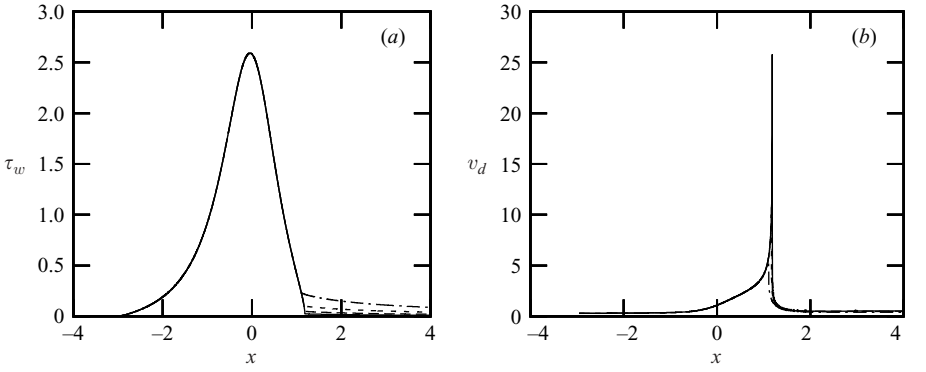

FIGURE 3. (*a*) Wall shear and (*b*) displacement velocity profiles corresponding to figure 2(*a*).

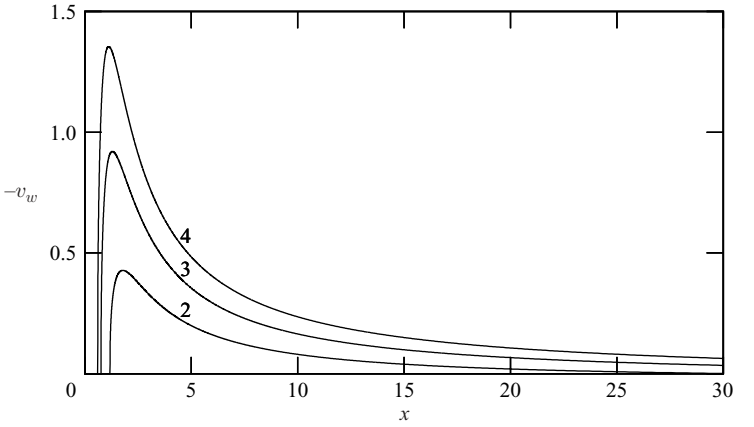

FIGURE 4. Suction profiles for $\Omega_m = 0.025$ and $a = 2$, 3, and 4.

The steady wall shear in figure 3(*a*) shows the effect of the suction as soon as the vorticity parameter drops below the preset level Ω_m. The displacement thickness rises downstream of the nose in all cases to meet the Blasius solution far downstream where $\delta^* \sim x^{1/2}$, but actual levels of δ^* are reduced at fixed x with increasing values of Ω_m. The displacement velocity v_d at the boundary-layer edge is shown in figure 3(*b*). A spike develops for $\Omega_m \to 0$ at the streamwise location where suction starts; note that the smaller the value of Ω_m, the later suction begins and the closer the solution is to infinite displacement velocity as a Goldstein singularity is approached. The heights of the spike shown in figure 3(*b*) probably converge with mesh size, but convergence is slow, especially at small Ω_m, and seems to depend on exactly where the streamwise mesh points happen to fall compared to the exact initiation of suction. Improved values of the spikes could possibly be found from an appropriate extrapolation based on the analytical structure near the initiation of suction. Lastly, the suction profiles for various values of a are shown in figure 4; for $a = 4$, the suction extends as far downstream as $x = 125$.

The case where suction is constant over a finite range, $i = 0$ in (2.8), has been studied by many authors and this second situation is also considered here. Since the separation singularity moves toward the nose with increasing a, it seems most reasonable to start the suction at $x_0 = 0$. In order to find the minimum suction volume under these

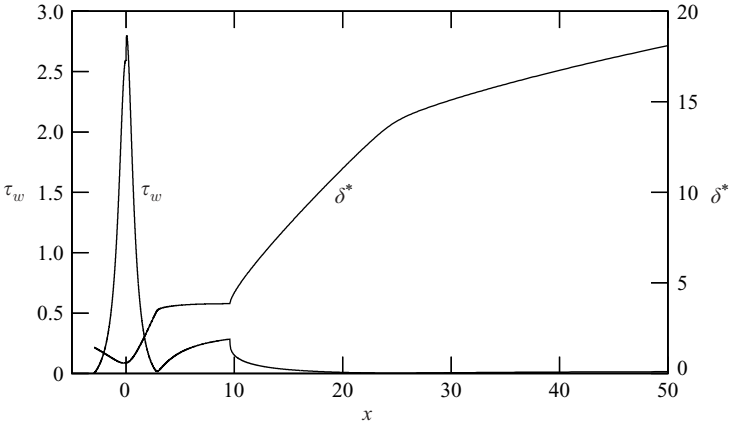

FIGURE 5. Wall shear and displacement thickness for $a = 2$ and uniform suction with $V = 0.303$ applied from $x = 0$ to 9.57.

two constraints, first the minimum suction velocity V was determined by trial and error, which produced an unseparated state when suction is extended downstream indefinitely (i.e. $x_1 \to \infty$). For example, for $a = 2$, the case shown in figure 5, it required a suction velocity $V = 0.303$ to keep the minimum shear at $x = 2.9$ positive. When the suction velocity was slightly reduced to $V = 0.302$, the minimum drops to zero and a Goldstein singularity forms. This result proved true for all meshes employed from 512^2 to 4096^2 and whether central x-differences with a smoothed velocity jump or a couple of backward Euler steps at an abrupt jump in suction was used at $x_0 = 0$.

With a suction velocity $V = 0.303$, separation at $x = 2.9$ is just avoided, but further downstream, the pressure gradient decreases, and at some point the boundary layer has recovered enough that the suction can be terminated without causing any further separation. To minimize the suction volume, the suction region should be terminated as soon as possible. Note however from equation (3.2) and figure 1 that at the termination of suction at $x = x_1$, the wall shear plunges proportional to $-(x - x_1)^{1/3}$. Separation will then occur downstream of the suction slot unless x_1 is sufficiently large. The smallest value of x_1 to avoid downstream separation was found using a binary search technique to be $x_1 = 9.57$. Hence the minimum suction volume is obtained at a suction velocity $V = 0.303$ and a slot extending to $x_1 = 9.57$, producing a suction coefficient equal to $C_Q = 2.9$ and the final wall shear and displacement thickness distributions of figure 5. Note that a true local minimum in suction volume has been obtained: V cannot be reduced because the solution would separate at $x = 2.9$; variations in x_1 play no part in that. And if the value of x_1 is reduced, keeping C_Q constant, the minimum shear at $x = 24.6$ in figure 5 (most evident from the relaxation of the displacement thickness growth after passing the region of marginal separation) separates. Far downstream, the wall shear approaches the Blasius value ($|\omega(x, 0)| \sim 0.332x^{-1/2}$) but very slowly; there is still a 30% error at $x = 200$, 20% at 400, 14% at 800 and 10% at 1700. Yet is seems clear that the Blasius value is indeed approached, ensuring that the suction found does indeed prevent separation for all x.

Calculated values for constant suction for other values of a are summarized in table 2. A comparison with table 1 shows that the suction coefficients for constant suction are larger than those for 'locally minimal suction', as conjectured. However the differences are not large and it appears that constant suction starting at the nose is relatively efficient. This result is in qualitative agreement with the experiments

a	V	x_1	C_Q
2	0.3026	9.57	2.90
3	0.6706	12.5	8.39
4	1.0002	17.2	17.2

TABLE 2. Minimum suction velocity and parameters for unseparated flow when $x_0 = 0$ and $i = 0$ in equation (2.8).

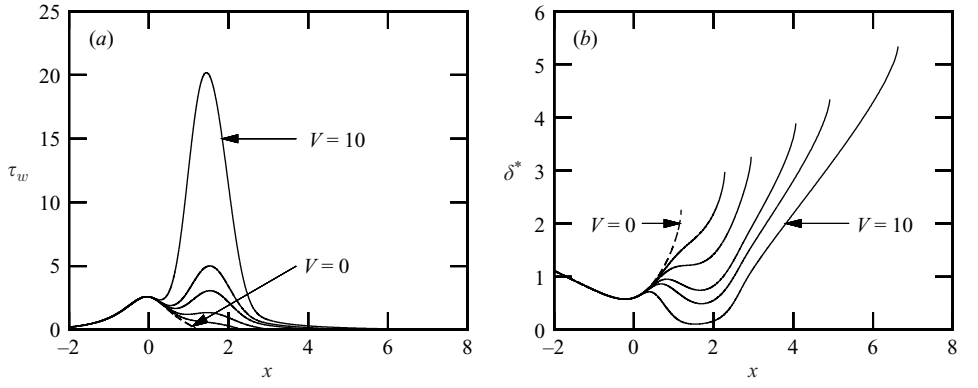

FIGURE 6. (*a*) Wall shear and (*b*) displacement thickness profiles for smooth suction, $i = 3$, between $x = 0$ and 2.9 at $a = 2$; peak suction velocities $V = 0$ (broken), 0.5, 1, 2, 3, and 10.

of Poppleton (1955) and the numerical simulations of Wang (1995). Lastly, since solid-wall separation occurs at $x = 1.1867$ for $a = 2$, it might seem worthwhile to try to save suction volume by starting the suction at say, $x_0 = 1$, instead of at the vertex $x_0 = 0$; however this modification changed the required suction velocity to 0.361 with $x_1 = 8.9$ and hence C_Q is almost the same.

In some experiments (see, for example, Alrefai & Acharya 1996), a narrow slot was used. To determine the effect of applying a larger suction velocity over a narrower slot, the suction velocity for $a = 2$ was raised from $V = 0.303$ to 1 with the start of suction moved to $x_0 = 1$, which is closer to the solid-wall separation location. It was found that suction had to then extend to $x_1 = 5.2$, giving a required suction coefficient $C_Q = 4.2$, which is significantly more than the value 2.9 in table 2. Hence at least in this case a smaller suction region requires a larger volumetric flow rate; this appears consistent with existing data such as Poppleton (1955) and Wang (1995). Note that when the slot is extended farther downstream, the average pressure at which the fluid is removed increases, decreasing average required pumping vacuum.

Next suction of the type (2.8) was considered with $i = 3$, $x_0 = 0$ and $x_1 = 2.90$ for various values of V. The wall shear and displacement thickness distributions for $a = 2$ are shown in figures 6(*a*) and 6(*b*), respectively, and the separation locations for various parameters in table 3. With increasing suction the separation point moves downstream of the end of the slot but for $a = 2$, despite the fact that suction coefficients considerably higher than 2.34 (see table 1) were used (up to 12.3), separation still occurs.

Since separation could be completely avoided using longer suction slots (for example those implied by figure 2(*a*) or those of table 2) this raises the question of whether a minimum slot size is needed if separation is to be avoided everywhere. It will be

$a\backslash V$	0	0.5	1	2	3	4	6	10
2	1.1867	2.2809	2.9434	4.0615	4.9263			6.6405
3	0.7661	0.8415		2.8239		3.6785	4.1033	4.4113
4	0.6079	0.6289	0.6564		2.8350		3.5488	3.8651

TABLE 3. Location of steady separation for smooth suction, $i = 3$, between $x_0 = 0$ and $x_1 = 2.9$.

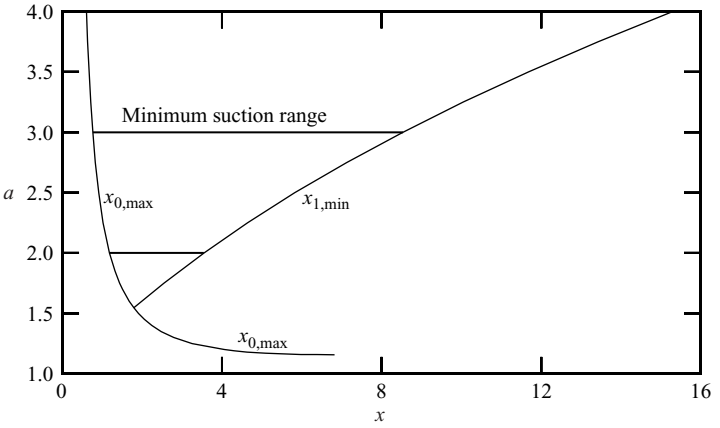

FIGURE 7. Minimum suction range required to prevent separation completely.

shown that this is indeed the case; in particular, for given a, the slot must at least extend over the range indicated in figure 7. For the indicated example, $a = 3$, the slot must start before $x = 0.766$ and must extend beyond $x = 8.54$. Otherwise, separation will occur even in the presence of large scaled suction through the slot.

Note that below a scaled angle of attack $a = 1.546$, where the two curves of figure 7 intersect, an arbitrarily narrow slot could be used, maybe located at $x = 1.79$, the intersection point. However, a finite scaled slot size is needed above this critical value.

Turning to the justification of these observations, the restriction on the starting point of the slot is simple: it is the location of separation for a solid wall (table 3 at $V = 0$). Since in the considered boundary-layer approximation, suction cannot affect the boundary-layer flow upstream of the slot, the slot must obviously start before the solid-wall separation location to avoid separation.

Conversely, if this requirement on the starting point is met, there will be no separation in the solid-wall boundary layer upstream of the slot. In addition, separation above the slot can be prevented by applying enough suction through the slot. In particular, for sufficiently large suction, u should approach an unseparated asymptotic suction profile having a displacement thickness that decreases and a wall shear that increases with increasing suction (Pretsch 1944). These trends are most evident in figures 6(a) and 6(b) near the centre of the slot; near the slot extremities the suction is relatively weak.

The second restriction, for the suction slot to extend at least as far downstream as the $x_{1,\min}$-curve in figure 7, is more complex. First consider the question of how soon the suction slot can be terminated assuming that the suction through the slot is very strong. If the suction is strong, the boundary layer above the slot is very thin (Pretsch

1944), and the boundary layer immediately behind the end of the slot has essentially zero thickness. The question of separation downstream of the slot then becomes that of whether a solid-wall boundary layer that starts at zero thickness at the end of the slot $x = x_1$ will separate for $x > x_1$. This question was answered using a modified code that resolved the initially infinitely thin boundary layer profile at x_1. It was found, using a binary search, that if x_1 was less than the values indicated by $x_{1,\min}$ in figure 7 (8.54 for the example $a = 3$), downstream separation occurs. Thus, for strong suction, the slot must extend past the limits shown in figure 7.

Note that there is another, vanishingly small, asymptotic region around x_1; however, since the pressure gradient is asymptotically negligible there, this region should only act to modify the shape of the thin profile from the asymptotic suction profile immediately upstream of x_1 to the Blasius profile just downstream.

One would reasonably expect that if the suction were less strong, the slot would need to be even larger than the limits of figure 7. This is certainly true for our examples of 'locally minimal' suction and minimal constant suction above. It is also in agreement with our other computational experiences. For example, figure 6(*b*) shows that as suction increases, separation is retarded (the infinite suction solution in this case predicts that the separation will reach $x = 9.76$ for infinite suction velocity V). Using the Pohlhausen approximation, it can be shown in general that the slots for finite suction velocity must be larger. This approximation produces an equation for $Z = \theta^2/\nu$ (Schlichting 1979, p. 210), where θ and ν are the momentum integral thickness and the kinematic viscosity, respectively, which can be cast in terms of a shape factor $K = U'_\infty \theta^2/\nu$ to obtain

$$\frac{U_\infty}{U'_\infty}\frac{\mathrm{d}K}{\mathrm{d}x} - \frac{U_\infty U''_\infty}{(U'_\infty)^2}K = F(K), \tag{4.2}$$

where $F(K)$ is a known function. In the region behind the slot, $U_\infty > 1$ and $U'_\infty < 0$ and consequently the differential equation (4.2) is regular and must have a unique solution. Separation occurs when K reaches the value -0.1567. Now suppose a suction slot is terminated at an x_1 before the position required according to figure 7. Then the boundary layer corresponding to strong suction, which starts at $K = 0$ at x_1, reaches separation, $K = -0.1567$, at some x_s. A boundary layer starting with finite thickness at x_1, corresponding to finite suction, has an initial K-value that is negative, hence is less than the infinite suction K-value. Going downstream, the K-values must stay below those of the infinite suction case, because if the two solution curves crossed, it would violate the uniqueness of the solution. That leaves no option but for the finite suction curve to reach separation, $K - 0.1567$, before the infinite suction curve does. And to still separate even when the limit of figure 7 is reached.

It should be pointed out that if the suction volumetric rate is raised sufficiently, in particular from $O(\varepsilon^2 Re_r^{-1/2})$ to $O(\varepsilon^2)$, for example, it becomes strong enough to have a significant effect on the external flow velocity and the present analysis is not valid. However, a suction volume much larger than the one required here would be a practical disadvantage.

5. Unsteady formulation

In practical applications of suction control, a slot of finite length is used and by adjusting the hole sizes or density in the wall various suction profiles at the surface can be produced. Here a profile of the form (2.8) was used with $i = 3$. To an extent, this is an arbitrary choice and was selected partly to ensure a relatively smooth

transition in boundary conditions at the slot edges in this first application of the Lagrangian method with suction.

The motion was taken to be impulsively started from rest, and for $t > 0$, an initially thin boundary layer forms on the parabola. To describe this phase of the motion in Eulerian coordinates, it is convenient to introduce the Rayleigh variable $\zeta = y/2\sqrt{t}$. The initial solution is $u = U_\infty(x)\mathrm{erf}(\zeta)$ for all x and ζ. It is convenient to introduce computational coordinates $\hat{x}$ and $\hat{\zeta}$ defined on the interval (0, 1) by

$$x - x_c = h_x(\hat{x}) = k_x \tan\left\{\pi\left(\hat{x} - \tfrac{1}{2}\right)\right\}, \quad \zeta = h_\zeta(\hat{\zeta}) = k_\zeta \tan\left(\tfrac{1}{2}\pi\hat{\zeta}\right). \tag{5.1}$$

The parameters k_x and k_ζ control the mesh spacing in physical space and x_c is a value of x around which the mesh is clustered. During the course of the work, clustering was carried out at several locations as discussed in § 7. A uniform mesh in computational space and smaller values of k_x and k_ζ imply more points concentrated near the point x_c and near the wall, respectively.

The solution of the transformed system (2.4) was advanced numerically forward in time from $t = 0$ using a Crank–Nicholson method with upwind-downwind differences for the first-order spatial derivatives (Doligalski & Walker 1984); the method is second-order accurate in space and time. The difference equations were solved using a simple alternating-direction-implicit (ADI) method, as opposed to the factored ADI method in Peridier *et al.* (1991). At any stage in the process, the streamfunction was evaluated by integration using Simpson's rule (Degani *et al.* 1996). The Rayleigh transformation was used only in the initial stages, when the boundary layer is thickening in physical space proportional to $t^{1/2}$. For large t the solution must approach the Blasius solution for large x and continued use of the Rayleigh variable causes the effective boundary layer in the computational domain to shrink toward the wall. Thus the computation was switched back to the y variable at a finite time t_d given in § 7. Let $\hat{y}$ denote a computational variable defined in an analogous way to equation (5.1); if the factor k_y is selected as $k_y = 2\sqrt{t_d}k_\zeta$, then mesh points in y and ζ match up and a return to the y variable can be made without interpolation.

6. Lagrangian method

For those values of a where separation occurs, the Eulerian calculation eventually fails to converge at a time denoted here by t_f. Thus at a selected time t_o well in advance of t_f, § 7, the calculation was restarted in Lagrangian coordinates.

As discussed by Cowley *et al.* (1990), once separation starts to develop, the boundary-layer flow starts to focus into an erupting plume which is very narrow in the streamwise direction. The phenomenon is characterized by a rapidly thickening boundary layer and strong local normal velocities. An effective way of dealing with this event is to introduce Lagrangian coordinates wherein the trajectories of a large number of fluid particles are evaluated. The main dependent variables are the streamwise particle positions and velocities x and u, respectively, which are functions of their initial positions (ξ, η) and t. The streamwise momentum equation takes the form (Van Dommelen & Shen 1982)

$$\frac{\partial u}{\partial t} = -\frac{\partial p_\infty}{\partial x} + \left\{-\frac{\partial x}{\partial \eta}\frac{\partial}{\partial \xi} + \frac{\partial x}{\partial \xi}\frac{\partial}{\partial \eta}\right\}^2 u, \quad \frac{\partial x}{\partial t} = u. \tag{6.1}$$

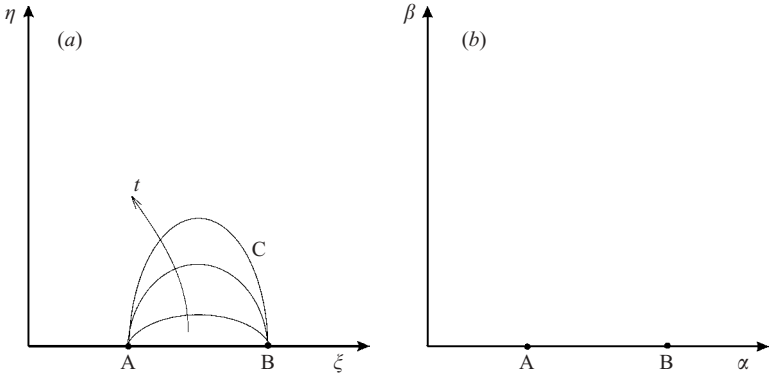

FIGURE 8. Schematic diagram of the solution domain in (*a*) Lagrangian space and (*b*) computational space.

At any instant, the normal particle positions $y(\xi, \eta, t)$ can be computed using the continuity equation in Lagrangian coordinates:

$$\frac{\partial x}{\partial \xi}\frac{\partial y}{\partial \eta} - \frac{\partial x}{\partial \eta}\frac{\partial y}{\partial \xi} = 1. \tag{6.2}$$

One important advantage of Lagrangian coordinates is that the occurrence of a separation singularity is unambiguously defined as the first instant when a stationary point occurs in the x field according to

$$\frac{\partial x}{\partial \xi} = \frac{\partial x}{\partial \eta} = 0 \quad \text{at} \quad \xi = \xi_s, \ \eta = \eta_s, t = t_s, \tag{6.3}$$

since these conditions make the solution of equation (6.2) singular; see Van Dommelen & Shen (1982) for details of the singularity structure. Note that the solution for x is believed to be regular even at separation (see, for example, Van Dommelen 1991). A Lagrangian integration may be initiated at any time t_o that the velocity field is a known function u_o of x and y, and initial conditions for the system (6.1), (6.2) are

$$x(\xi, \eta, t_o) = \xi, \quad y(\xi, \eta, t_o) = \eta, \quad u(\xi, \eta, t_o) = u_o(\xi, \eta). \tag{6.4}$$

When suction occurs through a slot between the points $x = x_0$ and $x = x_1$ on the wall, the slot location in Lagrangian space is a curve C, with end points A and B located at $(\xi, \eta) = (x_0, 0)$ and $(\xi, \eta) = (x_1, 0)$, which penetrates into the Lagrangian domain with the passage of time, as shown schematically in figure 8(*a*). The curve C represents the initial starting location of fluid particles which arrive at the slot at time t; at the start of the Lagrangian calculations $t = t_o$, the equation of C is simply $\eta = 0$. For an injection slot, the trend shown in figure 8(*a*) is analogous, except that C penetrates downward into the region $\eta < 0$. Note that v does not appear in the Lagrangian streamwise momentum equation and it is the movement of C in Lagrangian space that influences the solution for u. Because the problem involves a moving boundary, it is not convenient to carry out the calculation in the usual (ξ, η) coordinates. Instead, computational coordinates (α, β) are defined such that the slot remains on the α-axis between points A and B as indicated in figure 8(*b*).

There are a number of ways in which (α, β) can be defined; first consider a general mapping to computational space of the form

$$\alpha = \alpha(\xi, \eta, t), \quad \beta = \beta(\xi, \eta, t), \quad \tau = t - t_o, \tag{6.5}$$

with a corresponding inverse mapping

$$\xi = \xi(\alpha, \beta, \tau), \quad \eta = \eta(\alpha, \beta, \tau), \quad t = t_o + \tau. \tag{6.6}$$

Note that subsequent partial derivatives with respect to τ are taken with α and β held constant, while derivatives with respect to t are with ξ and η constant. Increments in computational space are given by

$$\begin{pmatrix} \mathrm{d}\alpha \\ \mathrm{d}\beta \\ \mathrm{d}\tau \end{pmatrix} = \begin{pmatrix} \alpha_\xi & \alpha_\eta & \alpha_t \\ \beta_\xi & \beta_\eta & \beta_t \\ 0 & 0 & 1 \end{pmatrix} \begin{pmatrix} \mathrm{d}\xi \\ \mathrm{d}\eta \\ \mathrm{d}t \end{pmatrix}, \tag{6.7}$$

where the subscripts denote partial differentiation and the quantities in the matrix give the metrics of the transformation. An analogous equation can be written for $(\mathrm{d}\xi, \mathrm{d}\eta, \mathrm{d}t)^T$, and upon comparing with equation (6.7), it is easily shown that

$$\begin{pmatrix} \alpha_\xi & \alpha_\eta & \alpha_t \\ \beta_\xi & \beta_\eta & \beta_t \\ 0 & 0 & 1 \end{pmatrix} = \frac{1}{\tilde{J}(\alpha, \beta, t)} \begin{pmatrix} \eta_\beta & -\xi_\beta & \xi_\beta\eta_\tau - \eta_\beta\xi_\tau \\ -\eta_\alpha & \xi_\alpha & \eta_\alpha\xi_\tau - \xi_\alpha\eta_\tau \\ 0 & 0 & \tilde{J} \end{pmatrix}, \tag{6.8}$$

where $\tilde{J} = \xi_\alpha\eta_\beta - \xi_\beta\eta_\alpha$ is the Jacobian of the transformation.

Denote the equation of C at any time in the Lagrangian plane by

$$\xi = \xi_w(\alpha, \tau), \quad \eta = \eta_w(\alpha, \tau), \tag{6.9}$$

and to determine the equations satisfied by ξ_w, η_w, suppose that fixed values of x_w and $y_w = 0$ on the slot in physical space are taken as fixed values of α and $\beta = 0$ in computational space (see figure 8), in other words:

$$x\,[\xi_w(\alpha, \tau), \eta_w(\alpha, \tau), t_o + \tau] = x_w(\alpha), \quad y\,[\xi_w(\alpha, \tau), \eta_w(\alpha, \tau), t_o + \tau] = 0. \tag{6.10}$$

Differentiation with respect to τ yields

$$\frac{\partial x}{\partial \xi}\frac{\partial \xi_w}{\partial \tau} + \frac{\partial x}{\partial \eta}\frac{\partial \eta_w}{\partial \tau} + \frac{\partial x}{\partial t} = 0, \quad \frac{\partial y}{\partial \xi}\frac{\partial \xi_w}{\partial \tau} + \frac{\partial y}{\partial \eta}\frac{\partial \eta_w}{\partial \tau} + \frac{\partial y}{\partial t} = 0, \tag{6.11}$$

where the partial derivatives of x and y are evaluated on the slot at $\xi = \xi_w$, $\eta = \eta_w$ at time $t_o + \tau$. In the most general case, where the suction is vectored (or the wall moves in the x-direction) with components specified as $u_w(x, t)$ and $v_w(x, t)$, substitution of

$$\frac{\partial x}{\partial t} = u_w(x_w(\alpha), t_o + \tau), \quad \frac{\partial y}{\partial t} = v_w(x_w(\alpha), t_o + \tau), \tag{6.12}$$

in equations (6.11) yields the governing relations for ξ_w and η_w:

$$\frac{\partial x}{\partial \xi}\frac{\partial \xi_w}{\partial \tau} + \frac{\partial x}{\partial \eta}\frac{\partial \eta_w}{\partial \tau} = -u_w, \quad \frac{\partial y}{\partial \xi}\frac{\partial \xi_w}{\partial \tau} + \frac{\partial y}{\partial \eta}\frac{\partial \eta_w}{\partial \tau} = -v_w. \tag{6.13}$$

These equations must be solved at any stage to determine the motion of the wall in Lagrangian space, subject to the initial conditions, from (6.4),

$$\xi_w = x_w(\alpha), \quad \eta_w = 0 \quad \text{at} \quad \tau = 0. \tag{6.14}$$

To evaluate the coefficients in equations (6.13), first note that in general

$$\frac{\partial x}{\partial \xi} = \frac{\partial x}{\partial \alpha}\frac{\partial \alpha}{\partial \xi} + \frac{\partial x}{\partial \beta}\frac{\partial \beta}{\partial \xi}, \quad \frac{\partial x}{\partial \eta} = \frac{\partial x}{\partial \alpha}\frac{\partial \alpha}{\partial \eta} + \frac{\partial x}{\partial \beta}\frac{\partial \beta}{\partial \eta}, \tag{6.15}$$

and using equations (6.8)

$$\frac{\partial x}{\partial \xi} = \frac{1}{\tilde{J}}\left\{\eta_\beta \frac{\partial x}{\partial \alpha} - \eta_\alpha \frac{\partial x}{\partial \beta}\right\}, \quad \frac{\partial x}{\partial \eta} = \frac{1}{\tilde{J}}\left\{-\xi_\beta \frac{\partial x}{\partial \alpha} + \xi_\alpha \frac{\partial x}{\partial \beta}\right\}. \tag{6.16}$$

Since x and u are evaluated in computational space as functions of (α, β, τ), then at any fixed τ, $\partial x/\partial\alpha$ and $\partial x/\partial\beta$ can be calculated on $\beta = 0$. Furthermore, once a particular mapping (6.5) is adopted, $\xi_\alpha, \xi_\beta, \eta_\alpha, \eta_\beta$ and $\tilde{J}$, can be evaluated on the slot. Also, differentiation of the second of equations (6.10) with respect to α yields

$$\frac{\partial y}{\partial \xi}\frac{\partial \xi_w}{\partial \alpha} + \frac{\partial y}{\partial \eta}\frac{\partial \eta_w}{\partial \alpha} = 0. \tag{6.17}$$

At any stage in the calculation $\partial\xi_w/\partial\alpha$ and $\partial\eta_w/\partial\alpha$ can be evaluated and consequently the continuity equation (6.2) and (6.17) are two equations in two unknowns for $\partial y/\partial\xi$ and $\partial y/\partial\eta$ evaluated on the slot. Thus equations (6.13) may be solved for the time derivatives of ξ_w and η_w and a numerical procedure to advance the solution for $\xi_w(\alpha, \tau)$ and $\eta_w(\alpha, \tau)$ in time can be developed.

Now consider the specific relation between ξ, η and α, β defined by

$$\xi(\alpha, \beta, \tau) = \xi_w(\alpha, \tau), \quad \eta(\alpha, \beta, \tau) = \eta_w(\alpha, \tau) + \beta, \tag{6.18}$$

so that the mesh lines are vertical in Lagrangian space with the wall defined by $\beta = 0$; in addition choose $x_w(\alpha) = \alpha$. Under this mapping

$$\xi_\alpha = \frac{\partial \xi_w}{\partial \alpha}, \quad \xi_\beta = 0, \quad \eta_\alpha = \frac{\partial \eta_w}{\partial \alpha}, \quad \eta_\beta = 1, \quad \tilde{J} = \frac{\partial \xi_w}{\partial \alpha}, \tag{6.19}$$

and the metrics can be evaluated from equation (6.8); from (6.14) and (6.18) $\tilde{J} = 1$ at the initiation of a Lagrangian calculation ($\tau = 0$). From (6.16)

$$\frac{\partial x}{\partial \xi} = \frac{1}{\tilde{J}}\left\{\frac{\partial x}{\partial \alpha} - \frac{\partial \eta_w}{\partial \alpha}\frac{\partial x}{\partial \beta}\right\}, \quad \frac{\partial x}{\partial \eta} = \frac{\partial x}{\partial \beta}, \tag{6.20}$$

where the right-hand sides are evaluated on $\beta = 0$, for α locations in the slot, when used in (6.13). For locations on the solid wall $\xi_w = \alpha$, $\eta_w = 0$ for all τ. Using (6.2) and (6.17)

$$\frac{\partial y}{\partial \xi} = -\frac{1}{x_\alpha}\frac{\partial \eta_w}{\partial \alpha}, \quad \frac{\partial y}{\partial \eta} = \frac{1}{x_\alpha}\frac{\partial \xi_w}{\partial \alpha}, \tag{6.21}$$

and x_α must be evaluated on the slot when (6.21) are used in the second of (6.13). Substituting (6.20) and (6.21) into (6.13), it follows that ξ_w and η_w satisfy

$$\frac{\partial \xi_w}{\partial \tau} = -\frac{u_w}{x_\alpha}\frac{\partial \xi_w}{\partial \alpha} + v_w x_\beta, \quad \frac{\partial \eta_w}{\partial \tau} = -\frac{v_w}{\partial \xi_w/\partial \alpha}\left\{x_\alpha - \frac{\partial \eta_w}{\partial \alpha}x_\beta\right\} - \frac{u_w}{x_\alpha}\frac{\partial \eta_w}{\partial \alpha}, \tag{6.22}$$

with x_α and x_β evaluated on the slot $\beta = 0$. Since $x = \alpha$ on $\beta = 0$ for all τ, equations (6.22) reduce to

$$\frac{\partial \xi_w}{\partial \tau} = v_w x_\beta, \quad \frac{\partial \eta_w}{\partial \tau} = -\frac{v_w}{\partial \xi_w/\partial \alpha}\left\{1 - \frac{\partial \eta_w}{\partial \alpha}x_\beta\right\}, \tag{6.23}$$

for $u_w = 0$, with x_β evaluated on $\beta = 0$.

Under the transformation (6.18), the boundary-layer equations (6.1) become

$$\frac{\partial u}{\partial \tau} + \alpha_t \frac{\partial u}{\partial \alpha} + \beta_t \frac{\partial u}{\partial \beta} = -\frac{\partial p_\infty}{\partial x} + \frac{\partial^2 u}{\partial y^2}, \quad \frac{\partial x}{\partial \tau} + \alpha_t \frac{\partial x}{\partial \alpha} + \beta_t \frac{\partial x}{\partial \beta} = u \tag{6.24}$$

where

$$\frac{\partial}{\partial y} = \frac{1}{\partial \xi_w/\partial\alpha}\left\{-\frac{\partial x}{\partial\beta}\frac{\partial}{\partial\alpha} + \frac{\partial x}{\partial\alpha}\frac{\partial}{\partial\beta}\right\}, \tag{6.25}$$

and the metrics α_t and β_t follow from equations (6.8) according to

$$\alpha_t = -\frac{\partial\xi_w/\partial\tau}{\partial\xi_w/\partial\alpha}, \quad \beta_t = \frac{1}{\partial\xi_w/\partial\alpha}\left\{\frac{\partial\eta_w}{\partial\alpha}\frac{\partial\xi_w}{\partial\tau} - \frac{\partial\xi_w}{\partial\alpha}\frac{\partial\eta_w}{\partial\tau}\right\}. \tag{6.26}$$

Because u and x, as well as the metrics α_t, β_t, are regular at separation, one of the main advantages of Lagrangian coordinates is preserved in the system (6.24)–(6.26).

Computational variables $\hat{x}$, $\hat{\alpha}$, $\hat{\beta}$, are defined by the first of (5.1) and

$$\alpha - x_c = h_\alpha(\hat{\alpha}) = k_x \tan\left\{\pi\left(\hat{\alpha} - \tfrac{1}{2}\right)\right\}, \quad \beta = h_\beta(\hat{\beta}) = k_y \tan\left(\tfrac{1}{2}\pi\hat{\beta}\right), \tag{6.27}$$

which have been chosen such that the Lagrangian mesh points match up with the Eulerian ones from § 5 at time t_o. Upon substitution into equations (6.24), it is easily shown that

$$\frac{\partial u}{\partial\tau} = -\frac{\partial p_\infty}{\partial x} + R\frac{\partial^2 u}{\partial\hat{\alpha}^2} + S\frac{\partial^2 u}{\partial\hat{\alpha}\partial\hat{\beta}} + T\frac{\partial^2 u}{\partial\hat{\beta}^2} + P\frac{\partial u}{\partial\hat{\alpha}} + Q\frac{\partial u}{\partial\hat{\beta}}, \tag{6.28}$$

$$\frac{\partial\hat{x}}{\partial\tau} + \frac{\alpha_t}{h'_\alpha(\hat{\alpha})}\frac{\partial\hat{x}}{\partial\hat{\alpha}} + \frac{\beta_t}{h'_\beta(\hat{\beta})}\frac{\partial\hat{x}}{\partial\hat{\beta}} = \frac{u}{h'_x(\hat{x})}, \tag{6.29}$$

where

$$\frac{R}{\Pi} = \left(\frac{\partial\hat{x}}{\partial\hat{\beta}}\right)^2, \quad \frac{S}{\Pi} = -2\frac{\partial\hat{x}}{\partial\hat{\alpha}}\frac{\partial\hat{x}}{\partial\hat{\beta}}, \quad \frac{T}{\Pi} = \left(\frac{\partial\hat{x}}{\partial\hat{\alpha}}\right)^2, \quad \Pi = \left\{\frac{h'_x(\hat{x})}{(\partial\xi_w/\partial\hat{\alpha})h'_\beta(\hat{\beta})}\right\}^2, \tag{6.30}$$

$$P = -\frac{\alpha_t}{h'_\alpha(\hat{\alpha})} + \Pi\left\{-\frac{\partial^2\xi_w/\partial\hat{\alpha}^2}{\partial\xi_w/\partial\hat{\alpha}}\left(\frac{\partial\hat{x}}{\partial\hat{\beta}}\right)^2 + \frac{\partial\hat{x}}{\partial\hat{\beta}}\frac{\partial^2\hat{x}}{\partial\hat{\alpha}\partial\hat{\beta}} - \frac{\partial^2\hat{x}}{\partial\hat{\beta}^2}\frac{\partial\hat{x}}{\partial\hat{\alpha}} + \frac{h''_\beta}{h'_\beta}\frac{\partial\hat{x}}{\partial\hat{\alpha}}\frac{\partial\hat{x}}{\partial\hat{\beta}}\right\}, \tag{6.31}$$

$$Q = -\frac{\beta_t}{h'_\beta(\hat{\beta})} + \Pi\left\{\frac{\partial^2\xi_w/\partial\hat{\alpha}^2}{\partial\xi_w/\partial\hat{\alpha}}\frac{\partial\hat{x}}{\partial\hat{\alpha}}\frac{\partial\hat{x}}{\partial\hat{\beta}} - \frac{\partial\hat{x}}{\partial\hat{\beta}}\frac{\partial^2\hat{x}}{\partial\hat{\alpha}^2} + \frac{\partial\hat{x}}{\partial\hat{\alpha}}\frac{\partial^2\hat{x}}{\partial\hat{\alpha}\partial\hat{\beta}} - \frac{h''_\beta}{h'_\beta}\left(\frac{\partial\hat{x}}{\partial\hat{\alpha}}\right)^2\right\}. \tag{6.32}$$

The prime denotes differentiation and using equations (6.23), the metrics are

$$\alpha_t = -v_w\frac{h'_x(\hat{x})h'_\alpha(\hat{\alpha})}{h'_\beta(\hat{\beta})\partial\xi_w/\partial\hat{\alpha}}\frac{\partial\hat{x}}{\partial\hat{\beta}}, \quad \beta_t = v_w\frac{h'_\alpha(\hat{\alpha})}{\partial\xi_w/\partial\hat{\alpha}}. \tag{6.33}$$

In computational space, equations (6.23) become

$$\frac{\partial\xi_w}{\partial\tau} = v_w\frac{h'_x(\hat{x})}{h'_\beta(\hat{\beta})}\frac{\partial\hat{x}}{\partial\hat{\beta}}, \quad \frac{\partial\eta_w}{\partial\tau} = -\frac{v_w h'_\alpha(\hat{\alpha})}{\partial\xi_w/\partial\hat{\alpha}}\left\{1 - \frac{h'_x(\hat{x})}{h'_\alpha(\hat{\alpha})h'_\beta(\hat{\beta})}\frac{\partial\eta_w}{\partial\hat{\alpha}}\frac{\partial\hat{x}}{\partial\hat{\beta}}\right\}. \tag{6.34}$$

Finally, defining $\hat{y}$ as in § 5, the continuity equation (6.2) transforms to

$$\frac{\partial\hat{x}}{\partial\hat{\alpha}}\frac{\partial\hat{y}}{\partial\hat{\beta}} - \frac{\partial\hat{x}}{\partial\hat{\beta}}\frac{\partial\hat{y}}{\partial\hat{\alpha}} = \frac{(\partial\xi_w/\partial\hat{\alpha})\,h'_\beta(\hat{\beta})}{h'_x(\hat{x})h'_y(\hat{y})}. \tag{6.35}$$

A singularity occurs in computational coordinates when

$$\frac{\partial\hat{x}}{\partial\hat{\alpha}} = \frac{\partial\hat{x}}{\partial\hat{\beta}} = 0 \quad \text{at} \quad \tau = \tau_s. \tag{6.36}$$

a	V	t_v	t_f	t_o	t_s	x_s	C_Q
2	0	–		4.5	5.82	1.20	0
	0.5	0.2	10.213	9.0	10.2	2.34	0.62
	1.0		13.956	12.0	13.7	2.98	1.23
	2.0		24.669	20.0	24.4	4.09	2.46
	3.0		35.094	30.0	35.0	4.96	3.69
	10.0		59.370	50.0	60.4	6.67	12.3
3	0	–		1.5	2.55	0.789	0
	0.5	0.2	3.286	2.8	3.24	0.865	0.62
	2.0		7.570	6.5	7.56	2.86	2.46
	4.0		12.082	10.0	12.1	3.71	4.92
	6.0		14.388	12.0	14.7	4.13	7.38
	10.0		16.261	14.0	16.5	4.44	12.3
4	0	–		1.10	1.62	0.637	0
	0.5	0.2	1.773	1.5	1.77	0.665	0.62
	1.0		2.005	1.75	1.99	0.684	1.23
	3.0		5.427	4.7	5.42	2.89	3.69
	6.0		7.846	6.8	7.90	3.58	7.38
	10.0		9.038	7.8	9.19	3.89	12.3

TABLE 4. Parameters associated with the calculations and results.

7. Numerical methods

For a given value of a greater than the critical value 1.1576, integrations were initiated at $t = 0$ in the Eulerian system as described in § 5; for a solid wall, the boundary layer will eventually separate for all such cases (Degani *et al.* 1996). Generally, it was found that suction should be started well in advance of the separation time t_{ss} for a solid wall; otherwise, the imposed suction is not as effective in delaying separation. A similar conclusion has been reached by Wang (1995) for flows at moderate Re_r. Unsteady separation is not located at the wall, but relatively far away from it on the boundary-layer scale. Thus at times close to separation, asymptotically large controls are needed at the wall to influence the forming separation. This was dramatically illustrated through a numerical example by Van Dommelen (1990). For these reasons, suction was started shortly after $t = 0$ at a time denoted by t_v, given in table 4. The values of the scale parameters in equations (5.1) were selected pragmatically, and typical values of $k_x = 2.3$ and $k_\zeta = 0.8$ were used (Degani *et al.* 1996). For cases $a = 2$, 3 and $a = 4$ the switch to the y variable was done at $t_d = 1$ and $t_d = 0.2$, respectively.

The majority of each calculation was done in the Eulerian formulation, which is more efficient than in Lagrangian coordinates. However, as separation begins to develop, the numerical solution process discussed in § 5 encounters convergence problems and eventually fails at a time denoted here by t_f. This behaviour has been well-documented in other studies of two-dimensional unsteady separation (Van Dommelen & Shen 1980, 1982; Cowley *et al.* 1990; Degani *et al.* 1996), and indicates the need to switch to the Lagrangian method; this was done at a time $t_o < t_f$, given in table 4. The value of t_o must be selected well in advance of t_f so that the Eulerian velocity field is free of the substantial numerical errors that develop near t_f. A number of mesh sizes and time steps were used as a check on the accuracy. With increasing a separation develops more rapidly, necessitating the use of smaller time steps. In a typical preliminary calculation, similar time steps were taken as in Degani

et al. (1996), ranging from $\Delta t = 0.001$ to 0.0001, with a (401×201) spatial mesh. All cases presented here are based on a final (601×301) mesh and are believed to be grid independent. In the Eulerian integration convergence at each time step was deemed to have occurred when the relative difference of two successive iterates for u agreed to within 10^{-6} at each mesh point.

In Lagrangian space, the mesh moves according to (6.18), and the new slot position in Lagrangian space must be computed by solving equations (6.34) at each time step. If the solution is known at time $\tau - \Delta\tau$ (the previous time plane), the objective is to advance the solution to the current time plane at τ. The $\hat{x}$ field was first advanced by approximating equation (6.29) at $\tau - \Delta\tau$ using a simple forward difference for $\partial\hat{x}/\partial\tau$ and central differences for the spatial derivatives. This is an explicit predictor phase and is first-order accurate in $\Delta\tau$. With estimates of $\hat{x}(\hat{\alpha}, \hat{\beta}, \tau)$ in hand, $\partial\hat{x}/\partial\hat{\beta}$ at $\hat{\beta} = 0$ was estimated at τ using a second-order sloping three-point difference. The first of equations (6.34) was then approximated at $\tau - \Delta\tau/2$ using a simple average in τ for the right-hand side and a central difference for $\partial\xi_w/\partial\tau$; this produces an estimate of $\xi_w(\hat{\alpha}, \tau)$ which is second-order accurate in space and time. Similarly, the solution for $\eta_w(\hat{\alpha}, \tau)$ was advanced to the current time plane, although on the first pass $\partial\eta_w/\partial\hat{\alpha}$ was estimated from the solution in the previous time plane. At this stage, estimates of $\hat{x}$, ξ_w and η_w are available, and the solution of equation (6.28) was advanced using a Crank–Nicholson method similar to that discussed in § 5; the coefficients in equation (6.28) were approximated with a simple average in τ and upwind differences were used for $\partial u/\partial\hat{\alpha}$ and $\partial u/\partial\hat{\beta}$, depending on the sign of P and Q respectively (Doligalski & Walker 1984). The resulting difference equations were then solved using a single pass of a simple ADI scheme, in which the mesh was swept in the $\hat{\alpha}$- and then the $\hat{\beta}$-direction. At this point $\hat{x}(\hat{\alpha}, \hat{\beta}, \tau)$ was refined by approximating equation (6.29) at $\tau - \Delta\tau/2$ in a corrector phase that yields a second-order estimate of the $\hat{x}$ field. Next the solutions of (6.34) and then (6.28) were refined. The process was iterated until successive estimates of u agreed to six significant figures at each point; typically, this required three global iterations per step.

The position of the slot penetrates the Lagrangian domain with increasing τ and, as an example, consider the situation shown in figure 9, where $\hat{\xi} = h_x^{-1}(\xi)$, $\hat{\eta} = h_y^{-1}(\eta)$, $a = 2$, $V = 1$, $t_o = 4$, $i = 2$ in (2.8), and the slot edges are at $\xi = 0, 2.90$. The position of the slot changes at later times as indicated. The derivatives $\partial\xi_w/\partial\hat{\alpha}$ and $\partial^2\xi_w/\partial\hat{\alpha}^2$ appear in equations (6.31)–(6.34), and the evolution of the corresponding physical quantities $\partial\xi_w/\partial\alpha$ and $\partial^2\xi_w/\partial\alpha^2$ are shown in figure 10 for the situation in figure 9. At the initiation of the Lagrangian integration at $\tau = 0$, $\partial\xi_w/\partial\alpha = 1$ and $\partial^2\xi_w/\partial\alpha^2 = 0$. The subsequent distribution of $\partial\xi_w/\partial\alpha$ is evidently continuous, but $\partial^2\xi_w/\partial\alpha^2$ develops growing discontinuities at the slot edges. To confirm this behaviour, consider the upstream edge of the slot at x_0 and assume that x_β remains continuous there; it follows from (2.8) and (6.23) that $\partial\xi_w/\partial\tau \sim (\alpha - x_0)^i$ just inside the slot edge while $\partial\xi_w/\partial\tau = 0$ upstream of the slot. Consequently, for $i = 2$, a discontinuity in $\partial^2\xi_w/\partial\alpha^2$ occurs at $\alpha = x_0$, hence in the coefficients of the equations being numerically integrated. This behaviour has potentially serious consequences if the integration continues for an indefinite period of time. A lengthy Lagrangian calculation is also undesirable from another standpoint. The position of the slot penetrates more deeply into the Lagrangian domain with the passage of time and inevitably this will result in an unacceptable skewness in the grid in Lagrangian space. The problem is manifested as an instability that develops in C (see figure 8) in the form of a point-to-point oscillation about a well-defined mean.

Finally in a lengthy Lagrangian calculation, fluid particles which were initially close to one another eventually become separated by large distances; consequently

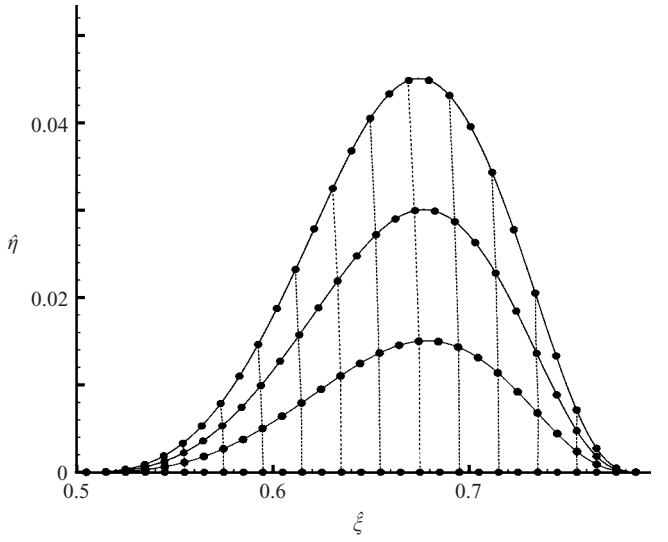

FIGURE 9. Penetration of the slot into the Lagrangian domain for a typical case $a = 2$, $i = 2$, $t = 4.0(0.1)4.3$; the dotted lines are the trajectories of selected wall mesh points originally at $\eta = 0$.

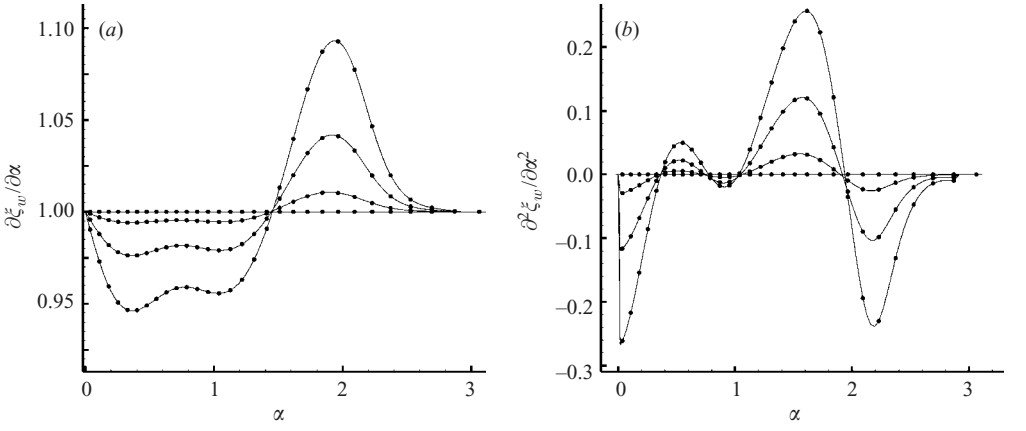

FIGURE 10. Gradients of ξ_w for the case shown in figure 9 at the same times.

gradients of $\hat{x}$ and $\hat{u}$ in (6.28)–(6.34) become large. The need for remeshing is signalled by a progressive rise in the global iterations required for convergence at a time step. The cure of these problems is periodical remeshing. The remeshing algorithm used here is similar to that of Degani, Walker & Smith (1998); briefly summarized, the continuity equation (6.35) is integrated along its characteristics to locate the new mesh points in the previous mesh.

In order to test the present Lagrangian methods, Eulerian calculations were run for specific cases up to a selected time t_t. The mesh clustering location x_c was initially chosen at the vertex of the parabola $x = 0$ as in Degani *et al.* (1996). The computation was then rerun by switching over to Lagrangian coordinates at an earlier time such as $t_t/2$ and a comparison of the Eulerian and Lagrangian results for wall shear (which is believed to be most sensitive to error) was made. Outside the slot, agreement was typically

$O(10^{-8})$ or smaller, while inside differences approaching 10^{-4} were seen, especially for cases with large suction magnitudes V. To enhance the comparison and gain confidence in the Lagrangian algorithm, several modifications were made. First the clustering location was shifted to the middle of the slot where streamwise variations in both suction velocity and pressure gradient are large. A second improvement concerned the remeshing process. The decision as to when to remesh is somewhat subjective. The initial criterion adopted was to evaluate $\hat{\eta}_w = h_y^{-1}(\eta_w)$ and once the maximum value exceeded 0.1, a remeshing was carried out. Depending on the value of V, remeshing is needed on the order of every 100 time steps or more. There is a potential loss in accuracy at each remeshing and to minimize this error, two actions were taken. First the bilinear interpolation formula used by Degani *et al.* (1998) was replaced by a third-order formula involving six points. Second, in order to reduce the number of remeshings, the criterion for a remeshing was changed so that the maximum of $\hat{\eta}_w$ had to exceed 0.5. Since the maximum possible value of $\hat{\eta}_w$ is 1, the penetration of the slot boundary in Lagrangian space is fairly deep; setting the criterion at larger values than 0.5 produced oscillations which were traced back to excessive mesh skewness in Lagrangian space. All changes were beneficial such that both computations agreed closely over a common time interval, even after several remeshes. Note that remeshing too close to the singularity time t_s is problematic and for this reason, the remeshing criterion was often relaxed as $t \to t_s$. Finally, suction was found to significantly weaken the separation process in some cases; such situations were encountered by Degani *et al.* (1998), where separation was dramatically inhibited by a moving wall. These cases are difficult to compute accurately since the computation continues for relatively long times in the Lagrangian frame; indeed separation was often so weak that Eulerian computations can be continued (with a coarse spatial mesh) through the separation event, illustrating the problems in Eulerian computations. In these cases the separation location was located approximately by a preliminary calculation. A refined computation was then carried out with the cluster point in α switched to the suspected separation point. This process was effective in accurately resolving the cases of 'weak separation'.

8. Calculated results

Computations were carried out for various combinations of slot widths, slot locations and suction characteristics. For a solid wall, a separation singularity occurs at times t_{ss} (listed in table 4 as t_s for $V = 0$) at locations x_s computed by Degani *et al.* (1996) and to be an effective separation control, suction must be applied near these locations. However separation can then occur downstream of the slot, and thus the slot should extend a reasonable length along the upper surface. After considerable experimentation (Kim 1999), the leading edge of the slot was selected at $x_0 = 0$. For most calculations reported here, the downstream edge of the slot was at $x_1 = 2.90$ and $i = 3$ in (2.8).

Results and parameters for the present calculations are listed in table 4. All cases considered ultimately terminate in a singularity, but it is evident that separation always is delayed to a later time and shifted downstream (compared to the solid wall). The unsteady separation locations are slightly downstream of those for the steady case in table 3 (cf. Van Dommelen & Shen 1980). As V increases, substantial increases in t_s occur as shown in figure 11: here, the separation time, scaled with respect to the solid-wall value t_{ss}, is plotted versus the suction strength for the three values of a. The broken lines are spline fits to the data and are presented only as a visual aid to distinguish clearly different values of a. The open symbols indicate cases

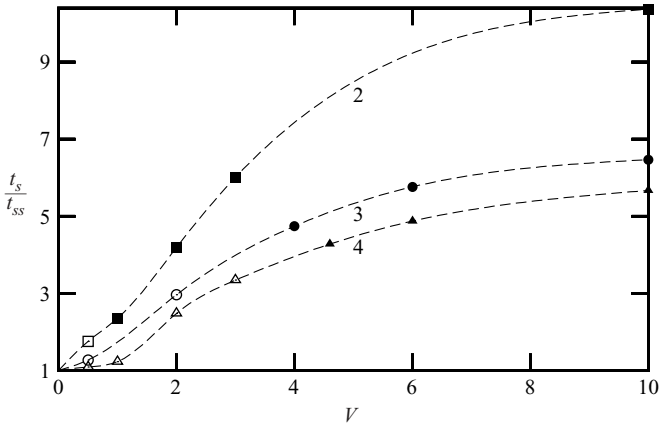

FIGURE 11. Calculated separation retardation by suction for $a = 2$, 3, and 4 versus V.

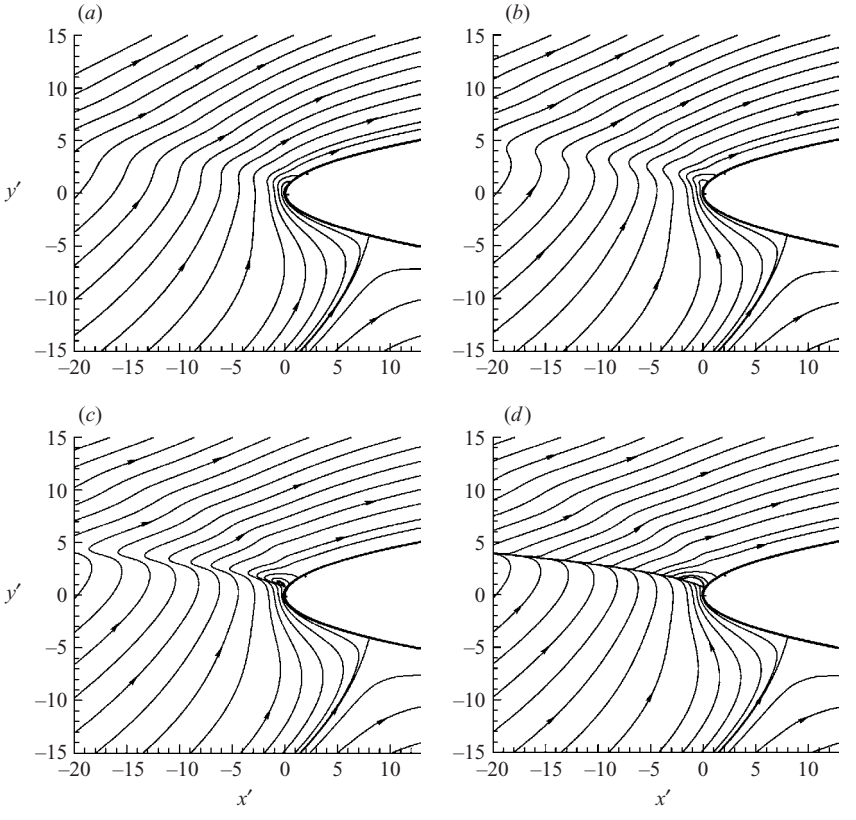

FIGURE 12. Instantaneous streamlines in the boundary layer for $a = 4$ and $V = 0.5$ at (*a*) $t = 0.5$, (*b*) $t = 1.0$, (*c*) $t = 1.5$, (*d*) $t = 1.7$.

in which the separation occurs above the suction slot, and solid ones behind the slot. The drop-off in effectiveness of suction at large V is related to the separation location moving downstream to regions where suction is weaker and eventually disappears.

The flow development for a typical case when the suction is weak is shown in figure 12. Note that this and subsequent figures are not at a realistic Reynolds

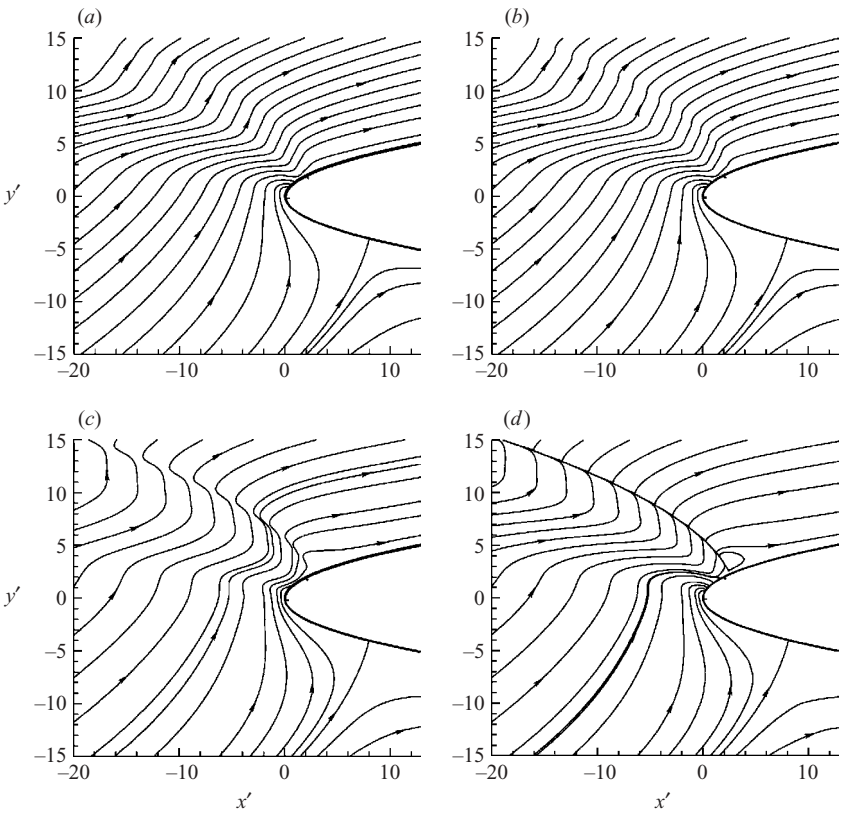

FIGURE 13. Instantaneous streamlines in the boundary layer for $a = 4$ and $V = 6$ at (*a*) $t = 2.0$, (*b*) $t = 4.0$, (*c*) $t = 7.0$, (*d*) $t = 7.9$.

number and show magnified instantaneous streamlines in a thin layer next to the parabola. The adverse pressure gradient for $a = 4$ is relatively severe and separation takes place for a solid wall near the leading vertex at $x_s = 0.637$. As indicated in table 4, separation occurs for $V = 0.5$ a little later and a little further downstream, but the modification of the process is only slight. In contrast, when the suction strength is increased, the evolution of a recirculation zone is delayed substantially as shown in figure 13; a recirculating eddy is not evident until just before $t = 7$ in figure 13(*c*). Separation eventually occurs at $t_s = 7.9$, which is about 5 times longer than for a solid wall. Now separation is suppressed above the slot but occurs on the solid wall downstream as shown in figure 13(*d*). This suggests that lengthening the slot downstream will produce a greater separation delay. To verify this point, calculations were also done with the slot end at $x_1 = 4$, and further delays proved possible provided that V was adjusted. If, for example, the same V is used, separation can actually occur above the slot at an earlier time. This happens because the peak in suction velocity is shifted downstream, resulting in a weakening of local suction near the leading edge, thereby permitting separation there. Calculated results for $a = 4$, $V = 14$ are shown in figure 14 for $x_1 = 4$. A singularity eventually occurs at $x_s = 5.85$ (downstream of the slot) at $t = 17.8$. Evidently, additional increases in the slot length could be used to further delay separation.

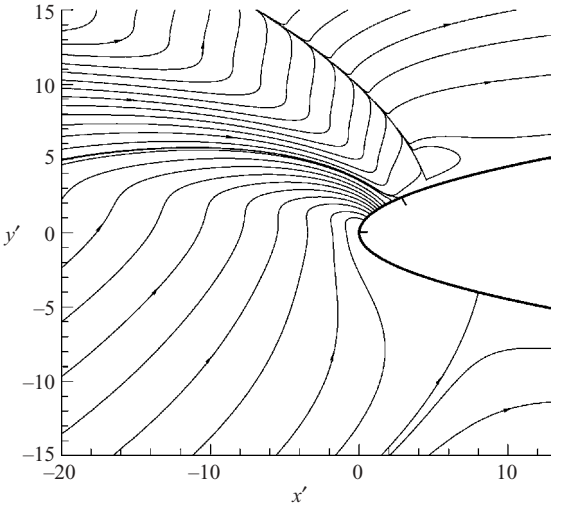

FIGURE 14. Instantaneous streamlines for $a = 4$, $x_1 = 4$ and $V = 14$ at $t_s = 17.8$.

Lastly, although the bulk of the results reported here used the suction distribution in (2.8) with $i = 3$, other calculations were done for other values of i but a qualitatively significant effect was not found. For example, for $C_Q = 7.38$, $a = 4$, which is a case shown in table 4 with $i = 3$, V must be altered from 6 to 5.1 for $i = 2$ to maintain the same suction volume. In this case, separation eventually occurred at $t_s = 8.54$ and $x_s = 3.73$, which are close to the values in table 4.

9. Concluding remarks

By extending the Lagrangian approach for computing unsteady separation to include a floating boundary, accurate numerical determination of unsteady separation in the presence of suction was possible. The present results show that the boundary-layer separation at high Re can be substantially inhibited using suction over a small slot near the leading edge of a thin airfoil. The physical suction velocity is $O(Re_r{}^{-1/2})$, and consequently the mass flow rates involved are not substantial. As shown in figure 11, for a slot occupying the first 3.3% of the chord (for a Joukowsky airfoil with thickness ratio 0.12), delays in separation of five to ten times are possible. Further delays are possible by lengthening the slot. This is consistent with the Navier–Stokes calculations of Wang (1995) for a Reynolds number based on chord length of 5000; the slot extended over the first 20% of the chord of a NACA 0012 airfoil, and it was found that separation from the leading edge could be suppressed entirely using a suction volume $C_Q = 28$ at $a = 5.88$ (30°). However, the applications of potential interest in this study are associated with rotorcraft and brief manoeuvres of combat aircraft. Suppression of leading-edge separation is desirable but inhibiting and weakening the process and shifting it downstream are also useful when the slot size or the volumetric flow rates involved in suction are a concern. Lack of space has been cited for the failure to extend the leading-edge suction on an F86-F to later fighters that had thinner wings (Flatt 1961), and similar concerns may apply to rotorcraft. The results obtained show that in the transient case, surprisingly large effects on separation, and consequently on aerodynamic forces, can be obtained by only slight amounts of suction through small slots, especially for brief intervals of time. For example, at a

scaled effective angle of attack $a = 2$, a scaled suction coefficient of only 0.62 almost doubles both the separation time and its distance away from the nose. This amount of suction is much smaller than the minimum amount of suction required to avoid separation completely, 2.34, which would also need to be applied by means of the lengthy and awkward distribution of figure 4.

During the final edits of this paper, J. D. A. Walker unexpectedly passed away. As a fluid dynamicist who deeply believed in the value of theoretical analysis, and the driving force behind this paper, he will be very much missed by us all.

The Lehigh authors would like to thank the Army Research Office for support under Grant No. DAAD19-99-1-0244, and L. v. D. thanks NASA support under Grant No. NAG1-01057.

REFERENCES

Acharya, M. & Metwally, M. H. 1992 Unsteady pressure field and vorticity production over a pitching airfoil. *AIAA J.* **30**, 403–411.

Alrefai, M. & Acharya, M. 1996 Controlled leading-edge suction for management of unsteady separation pitching airfoils. *AIAA J.* **34**, 2327–2336.

Cebeci, T., Khattab, A. K. & Stewartson, K. 1980 On nose separation. *J. Fluid Mech.* **97**, 435–454.

Collins, W. M. & Dennis, S. C. R. 1973 Flow past an impulsively started circular cylinder. *J. Fluid Mech.* **60**, 105–127.

Cowley, S. 1983 Computer extension and analytic continuation of Blasius expansion for impulsive flow past a circular cylinder. *J. Fluid Mech.* **135**, 389–405.

Cowley, S. J., Hocking, L. M. & Tutty, O. R. 1985 On the stability of solutions of the unsteady classical boundary-layer equations. *Phys. Fluids* **28**, 441–443.

Cowley, S. J., Van Dommelen, L. & Lam, S. T. 1990 On the use of Lagrangian variables in descriptions of unsteady boundary-layer separation. *Phil. Trans. R. Soc. Lond.* A **333**, 343–378.

Currier, J. M. & Fung, K.-Y. 1992 Analysis of the onset of dynamic stall. *AIAA J.* **30**, 2469–2477.

Degani, A. T., Li, Q. & Walker, J. D. A. 1996 Unsteady separation from the leading edge of a thin airfoil. *Phys. Fluids* **8**, 704–714.

Degani, A. T., Walker, J. D. A. & Smith, F. T. 1998 Unsteady separation past moving surfaces. *J. Fluid Mech.* **375**, 1–38.

Doligalski, T. L., Smith, C. R. & Walker, J. D. A. 1994 Vortex interactions with walls. *Annu. Rev. Fluid Mech.* **26**, 573–616.

Doligalski, T. L. & Walker, J. D. A. 1984 The boundary layer induced by a convected vortex. *J. Fluid Mech.* **139**, 1–28.

Elliott, J. W., Cowley, S. J. & Smith, F. T. 1983 Breakdown of boundary layers: (i) on moving surfaces; (ii) in semi-similar flow; (iii) in fully unsteady flow. *Geophys. Astrophys. Fluid Dyn.* **25**, 77–138.

Flatt, J. 1961 The history of boundary layer control research in the U.S.A. In *Boundary Layer Control, Vol. I* (ed. G. Lachmann), pp. 124–143. Pergamon.

Francis, M. S. 1995 X-31: An international success story. *Aerospace America* **33**, 22–32.

Francis, M. S. & Keesee, J. E. 1985 Airfoil dynamic stall performance with large amplitude motions. *AIAA J.* **23**, 1653–1659.

Goldstein, S. 1948 On laminar boundary-layer flow near a position of separation. *Q. J. Mech. Appl. Maths* **1**, 43–69.

Ham, N. D. 1968 Aerodynamic loading on a two-dimensional airfoil during dynamic stall. *AIAA J.* **6**, 1927–1934.

Karim, M. A. & Acharya, M. 1994 Suppression of dynamic stall vortices over pitching airfoils by leading-edge suction. *AIAA J.* **32**, 1647–1655.

Katz, J. & Plotkin, A. 1991 *Low-Speed Aerodynamics*. McGraw-Hill.

Kim, C.-Y. 1999 Unsteady separation phenomena in two- and three-dimensional boundary-layer flows. PhD thesis, Lehigh University.

LIGHTHILL, M. J. 1963 Introduction. Boundary layer theory. In *Laminar Boundary Layers* (ed. L. Rosenhead), pp. 46–72. Oxford University Press.

MCALISTER, K. W. & CARR, L. W. 1979 Water tunnel visualizations of dynamic stall. *Trans. ASME: J. Fluids Engng* **101**, 367–380.

MCCULLOUGH, G. B. & GAULT, D. E. 1951 Examples of three representative types of airfoil-section stall at low speeds. *Tech. Rep.* TN 2502. NACA.

PERIDIER, V. J., SMITH, F. T. & WALKER, J. D. A. 1991 Vortex-induced boundary-layer separation. Part 1. The unsteady limit problem $Re \rightarrow \infty$. *J. Fluid Mech.* **232**, 91–131.

POPPLETON, E. D. 1955 Boundary layer control for high lift by suction of the leading-edge of a 40 degree swept-back wing. *Tech. Rep.* RM 2897. ARC.

PRETSCH, J. 1944 Grenzen der Grenzschichtbeeinflussung. *Zt. Angew Math Mech.* **24**, 264–267.

ROSENHEAD, L. (Ed.) 1963 *Laminar Boundary Layers*. Oxford University Press.

RUBAN, A. I. 1981 Singular solution for boundary layer equations with continuous extension downstream of zero friction point. *Izv. Akad. Nauk SSSR, Mekh. Zhid. i Gaza* **6**, 42–49.

SCHLICHTING, H. 1979 *Boundary Layer Theory*, 7th edn. McGraw-Hill.

SEARS, W. R. & TELIONIS, D. P. 1975 Boundary-layer separation in unsteady flow. *SIAM J. Appl. Maths* **28**, 215–235.

SHIH, C., LOURENCO, L. M. & KROTHPALLI, A. 1995 Investigation of flow at leading and trailing edges of pitching-up airfoil. *AIAA J.* **33**, 1369–1376.

SHIH, C., LOURENCO, L. M., VAN DOMMELEN, L. L. & KROTHPALLI, A. 1992 Unsteady flow past an airfoil pitching at constant rate. *AIAA J.* **30**, 1153–1161.

SMITH, F. T. & STEWARTSON, K. 1973 On slot injection into a supersonic boundary layer. *Proc. R. Soc. Lond* A **332**, 1–22.

STEWARTSON, K., SMITH, F. T. & KAUPS, K. 1982 Marginal separation. *Stud. Appl. Maths* **67**, 45–61.

TERRILL, R. M. 1960 Laminar boundary layer flow near separation with and without suction. *Phil. Trans. R. Soc. Lond.* A **253**, 55–100.

VAN DOMMELEN, L. L. 1990 On the Lagrangian description of unsteady boundary-layer separation. Part 2. the spinning sphere. *J. Fluid Mech.* **210**, 627–645.

VAN DOMMELEN, L. L. 1991 Lagrangian description of unsteady separation. In *Vortex Dynamics and Vortex Methods* (ed. C. R. Anderson & C. Grungard). Lectures in Applied Mathematics, vol. 28, pp. 701–718. American Mathematical Society.

VAN DOMMELEN, L. L. & SHEN, S. F. 1980 The spontaneous generation of a singularity in a separating boundary layer. *J. Comput. Phys.* **38**, 125–140.

VAN DOMMELEN, L. L. & SHEN, S. F. 1982 The genesis of separation. In *Symposium on Numerical and Physical Aspects of Aerodynamic Flows* (ed. T. Cebeci), pp. 293–311. Springer.

VAN DYKE, M. 1956 Second-order airfoil theory including edge effects. *Tech. Rep.* TR 1274. NASA.

VAN DYKE, M. 1964 *Perturbation Methods in Fluid Mechanics*. Academic.

WAGNER, H. 1925 Über die Entstehung des dynamischen Auftriebs von Tragflächen. *Z. Angew. Math. Mech.* **5**, 7–35.

WALKER, J. D. A. & DENNIS, S. C. R. 1972 The boundary layer in a shock tube. *J. Fluid Mech.* **56**, 19–47.

WANG, S.-C. 1995 Control of dynamic stall. PhD thesis, Florida State University.

WERLE, M. J. & DAVIS, R. T. 1972 Incompressible laminar boundary layers on a parabola at angle of attack: a study of the separation point. *Trans. ASME.* E: *J. Appl. Mech.* **39**, 7–12.

WHITE, F. M. 1991 *Viscous Fluid Flow*, 2nd edn. McGraw-Hill.

YU, Y. H., LEE, S., MCALISTER, K. W., TUNG, C. & WANG, C. M. 1995 Dynamic stall control for advanced rotorcraft application. *AIAA J.* **33**, 289–295.

ZALUTSKY, K. 2000 Unsteady boundary-layer separation. PhD thesis, Lehigh University.